



# EDAP+ TN on Quality Assessment of NewSat/MSI

Author(s):   
**Sébastien Saunier**  
**Sultan Kocaman**  
Task 2 Team

Approval: DocuSigned by:  
**Kevin Halsall**  
95EFDDD4879A4CF...  
**Kevin Halsall**  
Task 2 Lead

Accepted:   
**Clément Albinet**  
EDAP+ Technical Officer

## AMENDMENT RECORD SHEET

The Amendment Record Sheet below records the history and issue status of this document.

ISSUE	DATE	REASON
0.1	29 June 2023	First draft for ESA and Satellogic review
0.1	15 October 2023	Up-issued following ESA comments
1.0	15 February 2024	Formal issue following review

## TABLE OF CONTENTS

<b>AMENDMENT RECORD SHEET</b> .....	<b>2</b>
<b>TABLE OF CONTENTS</b> .....	<b>2</b>
<b>1. EXECUTIVE SUMMARY</b> .....	<b>4</b>
1.1 References.....	4
1.2 Glossary.....	6
1.3 Cal/Val Maturity Matrices.....	8
<b>2. DATA PROVIDER DOCUMENTATION REVIEW</b> .....	<b>12</b>
2.1 Product Information.....	12
2.2 Metrology.....	15
2.3 Product Generation.....	17
<b>3. DETAILED VALIDATION – PRODUCT DOCUMENTATION AND PRODUCT FORMAT</b> .....	<b>18</b>
3.1 Introduction.....	18
3.2 Product documentation.....	18
3.3 Product Format evaluation.....	18
<b>4. DETAILED VALIDATION – IMAGE QUALITY</b> .....	<b>20</b>
4.1 Introduction.....	20
4.2 Visual Inspection.....	20
4.3 Modulation Transfer Function (MTF).....	31
4.4 Signal To Noise Ratio (SNR).....	39
4.5 Results Compliance.....	45
<b>5. DETAILED VALIDATION – GEOMETRY</b> .....	<b>47</b>
5.1 Introduction.....	47
5.2 Absolute Geolocation Accuracy.....	47
5.3 Temporal Geolocation Accuracy.....	50
5.4 Inter-band Registration Accuracy.....	56
5.5 Results Compliance.....	60
<b>6. DETAILED VALIDATION – RADIOMETRY</b> .....	<b>62</b>
6.1 Introduction.....	62
6.2 Absolute Calibration Accuracy.....	62
6.3 Temporal Stability.....	65
6.4 Results Compliance.....	69
<b>APPENDIX A NS MISSION</b> .....	<b>71</b>



<b>APPENDIX B</b>	<b>MISSION TEST DATASET .....</b>	<b>72</b>
<b>APPENDIX C</b>	<b>NS CONSTELLATION .....</b>	<b>73</b>
<b>APPENDIX D</b>	<b>NS / MSI INSTRUMENT SPECTRAL CHANNELS .....</b>	<b>74</b>
<b>APPENDIX E</b>	<b>74NS / MSI INSTRUMENT GEOMETRY .....</b>	<b>77</b>

## 1. EXECUTIVE SUMMARY

This Technical Note (TN) details the results of the (preliminary) mission data quality assessments (including geometric calibration, radiometric calibration and image quality) performed on a sample of products originated by a constellation of commercial Earth Observation (EO) optical satellites; the NewSat (NS) satellite operated by Satellogic company.

The aforementioned mission data quality assessments are performed in accordance with the assessment guidelines, detailed in [RD-2], that constitute the European Space Agency (ESA) Earthnet Data Assessment Project (EDAP+) Project's *EO Mission Data Quality Assessment Framework*. An important representation of the latter framework, constructed by the National Physical Laboratory (NPL), is what is known as *the summary maturity matrix and the detailed validation maturity matrix*. It is a diagrammatic summary of the following:

- **Documentation Review:** *the EDAP Optical team reviews materials (e.g. data and documentation) provided by the data provider or operator, some of which may not be publically available, or even the scientific community (e.g. published papers). The results are detailed in Section 3 (covering the first four columns of the maturity matrix).*
- **Detailed Validation:** *the EDAP Optical team performs data quality assessments (i.e. validation assessments), independently of any validation assessments performed by the data provider and / or operator. The results are reported in Section 4 and in the last column, 'Validation', of the maturity matrix).*

The above assessments are performed by the EDAP Optical team using the appropriate in-house and open-source ad-hoc scripts / tools.

It is important to note the purpose of the aforementioned framework is to ensure that the delivered commercial mission data is fit for purpose and that all decisions regarding the inclusion of the commercial mission as an ESA third party mission can be made fairly and with confidence.

### 1.1 References

The following is a list of reference documents with a direct bearing on the content of this proposal. Where referenced in the text, these are identified as [RD-n], where 'n' is the number in the list below:

- RD-1. EDAP.REP.001 Earth Observation Mission Quality Assessment Framework, Issue 2.2, December 2 2022.
- RD-2. EDAP.REP.002 Earth Observation Mission Quality Assessment Framework – Optical Guidelines, Issue 2.1, 31 October 2021.
- RD-3. SATELLOGIC IMAGERY PRODUCT GUIDE, Version 1.0, April 2023.
- RD-4. Metrology And Product Generation, Pre and Post Launch Calibration, Characterization and Imagery Product Processing, Version 1.0, April 2023.
- RD-5. E. Bueno, "GEOMETRY Calibration, validation and operation of NS Mark IV". Presentation of JACIE Conference, March 2023.

- RD-6. A. Pose, “Radiometric Calibration of NS Mark IV: A high resolution microsatellite constellation”, Presentation of JACIE Conference, March 2023.
- RD-7. F. Pignol, “Image resolution calibration, validation and operation of NS Mark IV, a high resolution multispectral micro satellite constellation”, Poster of VH RODA conference, November 2022.
- RD-8. Satellogic web site, “Best Data from Space: How We Attain Optimal Spatial Resolution Imagery”, last visit (April 2023) - <https://satellogic.com/2023/03/20/optimal-spatial-resolution-imagery/>
- RD-9. KARIOS Image Matching Tool: Software User Manual, EDAP+ SUM 01, Version 1, June 2023)
- RD-10. I2R Corp, “Spatial Resolution Digital Imagery Guideline” - last visit (April 2023) <https://www.i2rcorp.com/main-business-lines/sensor-hardware-design-support-services/spatial-resolution-digital-imagery-guideline>
- RD-11. USGS System Characterization Report on the Satellogic NS Multispectral Sensor. Open-File Report 2021–1030–L Version 1.1, April 2022
- RD-12. Zanoni, “IKONOS Signal-to-Noise Ratio Estimation”, March 25-27, 2002, JACIE Workshop, 2002 <https://ntrs.nasa.gov/search.jsp?R=20040004380>
- RD-13. Françoise Viallefont-Robinet, Dennis Helder, Renaud Fraisse, Amy Newbury, Frans van den Bergh, Donghan Lee, Sébastien Saunier.. Comparison of MTF measurements using edge method: towards reference data set. Optics Express, Optical Society of America, 2018, 26 (26), pp.33625-33648. (hal-02055611)
- RD-14. K. Kohm, “Modulation transfer function measurement method and results for the Orbview-3 high resolution imaging satellite.” Proceedings of ISPRS, Istanbul, Turkey (2004).
- RD-15. Valenzuela, A. Q. and J. C. G. Reyes. “Comparative Study of the different versions of the General Image Quality Equation.” Proceedings of ISPRS Annals of the Photogrammetry, Remote Sensing and Spatial Information Sciences (2019): 493-500.
- RD-16. Saunier, S.; Pflug, B.; Lobos, I.M.; Franch, B.; Louis, J.; De Los Reyes, R.; Debaecker, V.; Cadau, E.G.; Boccia, V.; Gascon, F.; et al. Sen2Like: Paving the Way towards Harmonization and Fusion of Optical Data. Remote Sens. 2022, 14, 3855. <https://doi.org/10.3390/rs14163855>
- RD-17. Bouvet, M.; Thome, K.; Berthelot, B.; Bialek, A.; Czapla-Myers, J.; Fox, N.P.; Goryl, P.; Henry, P.; Ma, L.; Marcq, S.; Meygret, A.; Wenny, B.N.; Woolliams, E.R. RadCalNet: A Radiometric Calibration Network for Earth Observing Imagers Operating in the Visible to Shortwave Infrared Spectral Range. Remote Sens. 2019, 11, 2401. <https://doi.org/10.3390/rs11202401>
- RD-18. H. Cosnefroy, M. Leroy, X. Briottet, Selection and characterization of Saharan and Arabian desert sites for the calibration of optical satellite sensors, Remote Sensing of Environ., Vol. 58, N°1, pp 101-114, 1996

<https://www.sciencedirect.com/science/article/abs/pii/S0034425795002111?via%3Dihub>

- RD-19. Saunier, Sébastien & Goryl, Philippe & Chander, Gyanesh & Santer, Richard & Bouvet, Marc & Collet, Bernard & Mambimba, Aboubakar & Kocaman, Sultan. (2010). Radiometric, geometric, and image quality assessment of ALOS AVNIR-2 and PRISM sensors. IEEE T. Geoscience and Remote Sensing. 48. 10.1109/TGRS.2010.2048714.  
[https://www.researchgate.net/publication/262804365\\_Radiometric\\_geometric\\_and\\_image\\_quality\\_assessment\\_of\\_ALOS\\_AVNIR-2\\_and\\_PRISM\\_sensors](https://www.researchgate.net/publication/262804365_Radiometric_geometric_and_image_quality_assessment_of_ALOS_AVNIR-2_and_PRISM_sensors)
- RD-20. M. Bouvet, "Intercomparison of multispectral imagers over natural targets," in Proc. IGARSS, Barcelona, Spain, 2007 <https://doi.org/10.1109/IGARSS.2007.4423390>
- RD-21. H. Murakami, T. Tadono, H. Imai, J. Nieke, and M. Shimada, "Improvement of AVNIR-2 Radiometric Calibration by Comparison of Cross-Calibration and Onboard Lamp Calibration," IEEE Trans. Geoscience and Remote Sensing, vol. 47, no. 12, pp. 4051–4059, Dec. 2009  
<https://www.researchgate.net/deref/http%3A%2F%2Fdx.doi.org%2F10.1109%2FTGRS.2009.2018118>
- RD-22. G. Chander, D. Meyer, and D. L. Helder, "Cross-calibration of the Landsat 7 ETM+ and EO ALI sensor," IEEE Transactions on Geoscience and Remote Sensing, vol. 42, no. 12, pp. 2821–2831, Dec. 2004 <https://ieeexplore.ieee.org/document/1369378>
- RD-23. K. J. Thome, "In-flight intersensor radiometric calibration using vicarious approaches," Post-Launch Calibration of Satellite Sensors, Edited by S. A. Morain and A. M. Budge, Balkema Publishers, Philadelphia, pp. 93-102, 2004  
[https://www.researchgate.net/publication/260182735\\_Inflight\\_Intersensor\\_Radiometric\\_Calibration\\_using\\_the\\_Reflectance-Based\\_Method\\_for\\_Landsat-Type\\_Sensors](https://www.researchgate.net/publication/260182735_Inflight_Intersensor_Radiometric_Calibration_using_the_Reflectance-Based_Method_for_Landsat-Type_Sensors)

## 1.2 Glossary

The following acronyms and abbreviations have been used in this Report.

AC	Across-track
AT	Along Track
ATBD	Algorithm Theoretical Basis Document
BRDF	Bidirectional Reflectance Distribution Function
CEOS	Committee on Earth Observation Satellite
CT	Cross Track
DEM	Digital Elevation Model
DIFF	image of difference
EDAP+	Earthnet Data Assessment Project
EO	Earth Observation
ESA	European Space Agency
ESF	Edge Spread Function
FAIR	Findable, Accessible, Interoperable and Reusable
FWHM	Full Width at Half Maximum

GCP	Ground Control Point
GNSS	Global Navigation Satellite System
GSD	Ground Sampling Distance
HABA	High Resolution Adjusted BRDF Algorithm
HR	High Resolution
IFOV	Instantaneous Field of View
IVOS	InfraRed and Visible Optical Sensors
KARIOS	Kanade-Lucas-Tomassi based Algorithm for Registration of Images from Observing System
L1	Level 1
L3	Level 3
LOESS	Locally Estimated Scatterplot Smoothing
LSF	Line Spread Function
MGRS	Military Grid Reference System
MSI	Multi Spectral Instrument
MTF	Modulation Transfer Function
NIR	Near InfraRed
NPL	National Physical Laboratory
NS	NewSat , NewSat
PICS	Pseudo Invariant Calibration Site
RCN	RadCalNet
RER	Relative Edge Response
RGB	Red Green Blue
RMSE	Root Mean Square Error
ROI	Region Of Interest
SBAF	Spectral Band Adjustment Factors
SNR	Signal to Noise Ratio
SSO	Sun Synchronous Orbit
TDS	Test Data Set
TN	Technical Note
TOA	Top Of Atmosphere
UAV	Unmanned Aerial Vehicle
USGS	United States Geological Survey
VAA	Viewing Azimuth Angle
VHR	Very High Resolution
VZA	Viewing Zenith Angle
WGCV	Working Group for Calibration and Validation

### 1.3 Cal/Val Maturity Matrices

#### 1.3.1 Summary Cal/Val Maturity Matrix

The Summary Calibration / Validation Maturity Matrix provides an overall summary of the quality assessment results (see Figure 1-1). Together they summarise the results of the Documentation Review and the Detailed Validation. The Validation Summary column is separated from the main table to make clear the results can come from multiple assessment sources.

Data Provider Documentation Review			Validation Summary	Key
Product Information	Metrology	Product Generation		Not Assessed
Product Details	Radiometric Calibration & Characterisation 	Radiometric Calibration Algorithm	Radiometric Validation Method	Not Assessable
Availability & Accessibility	Geometric Calibration & Characterisation 	Geometric Processing	Radiometric Validation Results Compliance	Basic
Product Format, Flags & Metadata	Metrological Traceability Documentation 		Geometric Validation Method	Good
User Documentation	Uncertainty Characterisation 	Mission-Specific Processing	Geometric Validation Results Compliance	Excellent
	Ancillary Data			Ideal
				 Not Public

Figure 1-1: Summary Matrix Cal/Val Maturity Matrix

### 1.3.2 Detailed Validation Cal/Val Maturity Matrix

The Detailed Validation Cal/Val Maturity Matrix (see Figure 1-2) is instrument-domain specific and provides a more complete report of the analysis behind the Validation Summary – breaking down the validation methodologies used and the results. This section is aimed at the more technically focused reader.

A summary of EDAP validation results is listed below in Table 1-1 for what concerns the geometric assessment and sensor spatial resolution. For all items, results comply with vendor specifications and the grade for results compliance is Excellent. In particular for the geometric assessment, evaluated products are within the claimed accuracy specification.

The grade “Ideal” is never reached for the following reasons:

- There are extreme values, considered as algorithm limitations by the data provider and that should be better tracked and documented.
- There are errors introduced to the orthoimages caused by the Digital Elevation Model (DEM) and/or reference images.
- Band to band registration is degraded when it involves images from the Near InfraRed (NIR) channel.
- The image quality varies a lot within the constellation and it should be better documented within the product format itself.

Geometric Validation			Key
	Method	Results Compliance	
Sensor Spatial Resolution (MTF)	Knife Edge [RD-13]	0.1@Nyq	Excellent
Absolute Positional Accuracy	KARIOS Tool <sup>1</sup> and Raster Reference	10.0 m CE90	Excellent
Band-to-band Registration	KARIOS Tool	0.3 pixel	Excellent
Temporal Stability	KARIOS Tool	10.0 m CE90	Excellent

Figure 1-2: Geometric Validation Cal/Val Maturity Matrix

Regarding radiometric calibration including Signal to Noise Ratio (SNR), a summary of EDAP validation results is listed in

<sup>1</sup> Kanade-Lucas-Tomassi based Algorithm for Registration of Images from Observing System (KARIOS), [RD-9]

Table 1-2. As for geometry, the EDAP grade ‘Excellent’ is reached. Variability of calibration across the constellation is observed, in addition to the variability of noise within the image.

**Table 1-1: Geometric Validation Results**

	Inter-band Mean Accuracy [m], (#7 Products)	Absolute Geolocation Mean Accuracy [m], (#1 product)	Temporal Geolocation Mean Accuracy [m], (#7 products)
EDAP+	Green-Blue: 0.33 RMSE / <b>0.52</b> CE90 Green-Red: 0.29 RMSE / <b>0.49</b> CE90 Green-NIR: 0.49 RMSE / <b>0.78</b> CE90	1.17 RMSE <b>1.74</b> CE90	3.53 RMSE 4.73 CE90
Satelogic [RD-5],	Current performance: < <b>0.70</b> CE90 (Target: 0.3)	<i>Current performance</i> < <b>11.8</b> CE90 (Target: 10 m)	<i>Not available</i>
USGS results as report in [RD-11].	Green-Blue 0.06 RMSE/ <b>0.09</b> CE90 Green-Red 0.07 RMSE/ <b>0.10</b> CE90 Green-NIR: <i>0.19 RMSE/ 0.29 CE90</i>	<i>7.09 RMSE / 10.77 CE90</i>	<i>Not available</i>

**Table 1-2: Radiometric Validation Results**

Radiometric Validation		
	Method	Results Compliance
Absolute Calibration	RadCalNet based method	<10%
Signal to Noise	[RD-12] Statistics	100 @ rho=0.5

Key
Not Assessed
Not Assessable
Basic
Good
Excellent
Ideal
 Not Public

Temporal Stability	Pseudo Invariant Calibration Site (PICS) Pseudo Invariant Calibration Site based method (Sentinel-2 as reference)	No input from Satellogic <sup>2</sup>
--------------------	---	---------------------------------------

**Figure 1-3: Radiometric Validation Cal/Val Maturity Matrix**

A set of NS 10 images (referred to as “SN”10 in the filename and in this report) was previously assessed by the United States Geological Survey (USGS) as reported in [RD-11]. The dataset included two Level 1 (L1) products observed over Fes (Morocco) and Railroad Valley (Nevada) in 2021. In addition to geometric results listed in Table 1.1, comparing with EDAP+ results, the USGS report raises the following observations:

- The absolute radiometric calibration is estimated to be within [5% – 15 %], it is fully in agreement with EDAP results.
- The absolute / multi temporal geolocation accuracy results are pessimistic compared to EDAP ones. It might be due to method and also to product maturity (EDAP Test Data Set (TDS) is dated end of 2022).
- The inter-band accuracy results were better compared to the EDAP results, on the other hand, EDAP processing is based on a more representative dataset.

Regarding quality control of geometry (applied by the USGS team); absolute accuracy results are from two methods; “Ground Control Point (GCP)” and “Image matching”. Image matching method involves a comparison between Sentinel-2 / Multi Spectral Instrument (MSI) and NS image grids. Due to the lower accuracy of Sentinel-2 (3.0 m), these results are a good indicator of NS geolocation accuracy but cannot form a good basis to fully characterise NS internal image accuracy.

---

<sup>2</sup> The “No input from Satellogic” classification has been given as it was not possible to compare our results against an accuracy specification. However, based on the methodology used, the calculated calibration accuracy is mostly below 4%, which would classify as “Excellent”.

## 2. DATA PROVIDER DOCUMENTATION REVIEW

### 2.1 Product Information

This section covers a review of top-level product descriptive information, product format, and the supporting documentation.

The table below details general product information for NS. It is worth noting that parameters are documented either in the user products itself or in the supporting documentations. Aside from a classic L1 product, the delivered product also embeds a Level 3 (L3) dedicated to visual interpretation.

Product Details	
Grade: Good	
Justification	<p>There is a minimum set of information available in the product format but relevant information is mostly available in the user guide.</p> <p>In the product format, there is no information on the measurement data quality.</p> <p>Furthermore, any required and recommended information, including point of contact and product locator, is missing.</p>
Product Name	Level 1b, Level 1 micro, Level 1 and Level 3 products.
Sensor Name	MSI
Sensor Type	2D frame array, Optical instrument, Multichannel imager
Mission Type	The Aleph-1 constellation includes 33 NS Mark IV / Mark V3 satellites (as of April 2023). The company planned to expend its constellation over 200 satellites by 2025.
Mission Orbit	The orbit type is Sun Synchronous Orbit ( <b>SSO</b> ), with Inclination about 97.4°, Perigee 405.5 km
Product Version Number	<p>The product version is not directly indicated with metadata files.</p> <p>Each scene contains a unique identifier, transparent for the user, to ensure traceability. The software version is indicated but with no detail on configuration used.</p>
Product ID	{ObservationDate}_{ObservationTime}_SN{satelliteNumber} Where ObservationTime is the UTM Time, hour, minute, second.
Processing level of product	Ortho Rectified 1-meter Bundle: Level 1, Level 3 Ortho Rectified 70-centimeter Bundle: Level 1 SR, Level 3 SR
Measured Quantity Name	Spectral Radiance
Measured Quantity Units	W sr-1 m-2 nm-1 (SI)
Stated Measurement Quality	Stated to be within 10% radiometric accuracy
Spatial Resolution	The Ground Sampling Distance ( <b>GSD</b> ) depends on the satellite altitude and the off-nadir angle. The pixel size of L1 / L3 ortho products and L1 / L3 super resolution (ortho products) is 1.0 m and 0.7 m, respectively.

<sup>3</sup> <https://news.satnews.com/2022/03/13/five-new-satellites-from-satellite-to-launch-onboard-the-spacex-transporter-4-mission>

Spatial Coverage	<p>The spatial coverage is given in the JSON file with the geographical coordinates of the product footprint (corners).</p> <p>(For information, the image size of one basic scene (one camera) is about 5250 pixels x 1080 pixels (image width / image height), applicable for multispectral and panchromatic data.)</p>
Temporal Resolution	<p>The temporal resolution of the constellation is up to four acquisitions daily. The target is observed by using different satellites, different operational configuration (off nadir pointing up to 25°). Moreover each satellite is phased differently (equatorial crossing local time differs greatly).</p>
Temporal Coverage	<p>The temporal coverage is related to the duration of the constellation and is not related to the lifetime of one satellite. As shown in APPENDIX C, the first satellite launched in June 2017, is still in operation.</p> <p>The mean lifetime of one satellite is about 3 years.</p>
Point of Contact	<p><a href="https://satellogic.com/contact/">https://satellogic.com/contact/</a></p>
Product locator (DOI/URL)	
Conditions for access and use	
Limitations on public access	

### Availability & Accessibility

Grade: Good

Justification	<p>The data set meets many of the Findable, Accessible, Interoperable and Reusable (<b>FAIR</b>) Principles but there is no data management plan.</p>
Compliant with FAIR principles	Yes
Data Management Plan	No
Data Availability Status	To be confirmed

### Product Format, Flags and Metadata

Grade: Good

Justification	<p>The data product includes encoded GeoTiff images together with several metadata files; XML ISO 19115-2 metadata file, STAC GeoJSON files. Additional per pixel metadata as cloud mask and geometry information are also delivered.</p> <p>The data product format is well documented [RD-3] but not all fields are documented. The data product format meets scientific community naming conventions / standards. A comprehensive set of metadata and data flags are provided with risk of having duplicate information exposed within different files (XML, JSON).</p> <p>The compliancy to CARD4L-requirements is not relevant herein because Satellogic does not deliver surface reflectance product.</p>
Product File Format	<p>GeoTIFF Image (v 1.1)</p> <p>Metadata embedded within XM, JSON, GeoJSON (STAC 1.0.0-rc.2) files.</p>

Metadata Conventions	ISO 19115-2
Analysis Ready Data?	No

User Documentation		
Grade: Basic		
Justification	<p>The Satellogic user guide [RD-3] exists, and a lot information exists on the web (<a href="https://satellogic.com/">https://satellogic.com/</a>).</p> <p>Limited ATBD-type information is available and there is no document from alternative sources (peer review papers), except a few presentations performed during conferences (JACIE, VH-RODA etc.). Furthermore, there is no regular reporting about mission / constellation performance.</p>	
<i>Document</i>	<i>Reference</i>	<i>QA4ECV Compliant</i>
Product User Guide	[RD-3]	No
ATBD	N/A	N/A

## 2.2 Metrology

The metrological traceability chain has not been documented and so for this reason the EDAP grade for **Metrological Traceability Documentation** is 'Not Assessable'.

Radiometric Calibration & Characterisation	
Grade: Good	
Justification	<p>Pre-launch radiometric calibration &amp; characterisation activities are well documented in [RD-4] including set up of pre-launch radiometric budget.</p> <p>Within the same document, post-launch radiometric calibration activities are also documented but it does not include important aspects of sensor behaviour (relative radiometry, stability).</p> <p>Regarding absolute calibration, the operational approach of the Satellogic team relies on vicarious calibration in situ measurement (usage of RadCalNet (<b>RCN</b>) and inter calibration with "gold" standard sensors (i.e. Sentinel 2).</p> <p>Uncertainties of both methods are not discussed, and it is difficult to judge if all aspects of sensor behaviour are taken into account (sensitivity to cross track pointing, spectral definition).</p> <p>It is worth noting that post launch calibration and post launch validation are performed independently. The periodicity of these activities is not documented.</p>
References	<ul style="list-style-type: none"> <li>[RD-4], [RD-6], [RD-7], [RD-8]</li> </ul>
Geometric Calibration & Characterisation	
Grade: Good	
Justification	<p>Geometric calibration &amp; characterisation covers most important aspects of instrument behaviour at a level of quality to be judged fit for purpose.</p> <p>Information on calibration methods and post-launch characterisation is not available. Measurements needed to assess uncertainties at the component level and their impact on the final product are not included in the products.</p>
References	<ul style="list-style-type: none"> <li>[RD-4], [RD-5]</li> </ul>
Metrological Traceability Documentation	
Grade: Not Assessable	
Justification	No traceability chain discussed in the referenced document.

References	<ul style="list-style-type: none"> <li>[RD-4]</li> </ul>
------------	--

Uncertainty Characterisation	
Grade: Basic	
Justification	<p>Uncertainty established by limited comparison to measurements by other sensor/s.</p> <p>Sources of uncertainty are not sufficiently defined. Uncertainty per pixel is not given.</p>
References	<ul style="list-style-type: none"> <li>[RD-4], [RD-5]</li> </ul>

Ancillary Data	
Grade: Basic	
Justification	<p>Ancillary data used in product generation, specified to some extent, though incomplete. Not entirely of a sufficient quality to be judged “fit for purpose” in terms of the mission’s stated performance.</p> <p>The information on ancillary data is not provided with details (raster reference, DEM).</p>
References	<ul style="list-style-type: none"> <li>[RD-4], [RD-5]</li> </ul>

## 2.3 Product Generation

Radiometric Calibration Algorithm	
Grade: Not assessable	
Justification	No ATBD type information
References	N/A

Geometric Processing	
Grade: Not Assessable	
Justification	No ATBD type information
References	N/A

Mission-Specific Processing	
Grade: Not Assessable	
Justification	Cloud masking / Super Resolution Algorithm for which no documentation exists (No ATBD type information)
References	N/A

### 3. DETAILED VALIDATION – PRODUCT DOCUMENTATION AND PRODUCT FORMAT

#### 3.1 Introduction

Considering the innovative and often challenging technology associated with Very High Resolution (VHR) and High Resolution (HR) data, this section documents the results of the performed quality assessments with respect to the following validation aspects:

- Product Documentation
- Product Format Evaluation

#### 3.2 Product documentation

The below list provides status information on documentation:

- Product Format exists and information is included in the user guide;
- There is no existing Algorithm Theoretical Basis Document (ATBD);
- There is a draft User Guide;
- There is no Product Handbook;
- Several technical documents are available on the Satellogic site.

#### 3.3 Product Format evaluation

The delivered Ortho Scene Product (Level 1 / Level 3) embeds a set of metadata files and one folder ('rasters') into which images are stored. As mentioned in the user guide document, the structure is as follows:

- Level 1 Image - orthorectified, multispectral including Blue, Green, Red and NIR channel images. Radiometric corrections applied to correct for any sensor artefacts and transformation to top-of-atmosphere reflectance (GeoTIFF (512 x 512) format, Encoding Type UInt16)
- Level 3 Image - orthorectified, multispectral BGR. Image enhanced, for visual interpretation (GeoTIFF (512 x 512) format, Encoding Type Byte)
- Cloud Mask image express within the same geographic system as Level 1 / Level 3 images (GeoTIFF format, Encoding Type Byte).

Metadata

- Inconsistencies between information in the XML File (ISO 19115-2:2019<sup>4</sup>) and JSON Metadata STAC File (DoNetStac 1.0.0-rc-2<sup>5</sup>)

<pre> &lt;gmd:illuminationElevationAngle&gt;   &lt;gco:Real&gt;71.53991485840183&lt;/gco:Real&gt; &lt;/gmd:illuminationElevationAngle&gt; &lt;gmd:illuminationAzimuthAngle&gt;   &lt;gco:Real&gt;26.417828956840744&lt;/gco:Real&gt; &lt;/gmd:illuminationAzimuthAngle&gt; </pre>	<pre> view:sun_elevation: 71.53991485840 view:off_nadir: 26.41782895684 </pre>
XML File	Metadata STAC

<sup>4</sup> <https://www.iso.org/fr/standard/67039.html>

<sup>5</sup> <https://www.nuget.org/packages/DoNetStac/1.0.0-rc.2>



The format of imagery files (including mask data) is GeoTIFF. The metadata format is JSON.

## 4. DETAILED VALIDATION – IMAGE QUALITY

### 4.1 Introduction

The image quality analysis includes the following topics:

- Visual Inspection – Image Interpretability – Cloud Mask
- Modulation Transfer Function (**MTF**)
- SNR

### 4.2 Visual Inspection

Visual inspection was carried out over the Ankara test site and the image quality was evaluated with respect to Unmanned Aerial Vehicle (**UAV**) data (Figure 4-1 to Figure 4.5) and with respect to similar VHR images observed with Maxar and Pleiades missions (Figure 4-6 to Figure 4-9).

Regarding the method, the UAV orthophoto was down-sampled to 1 m using cubic spline resampling prior to comparison. Cubic spline interpolation was applied to obtain a smooth image output. SN30 L1 and L3 images from 22.02.2023 over the Ankara test site were compared with the UAV.

The contrast of L1 image was enhanced with histogram stretching using standard deviations ( $\pm 4\sigma$ ). No contrast enhancement was applied to L3 data. The Maxar MS orthoimage with 60 cm GSD taken on 13.10.2020 and Pleiades 50 cm pan-sharpened ortho taken on 12.05.2021 over Ankara test site. The contrast of both images was enhanced with histogram stretching using standard deviations ( $\pm 4\sigma$ ).

In all comparisons, we observed colour artefacts due to moving objects (Figure 4-1 and Figure 4-6). This artefact is associated with the focal plane arrangement and does not exist in Pleiades and Maxar images.

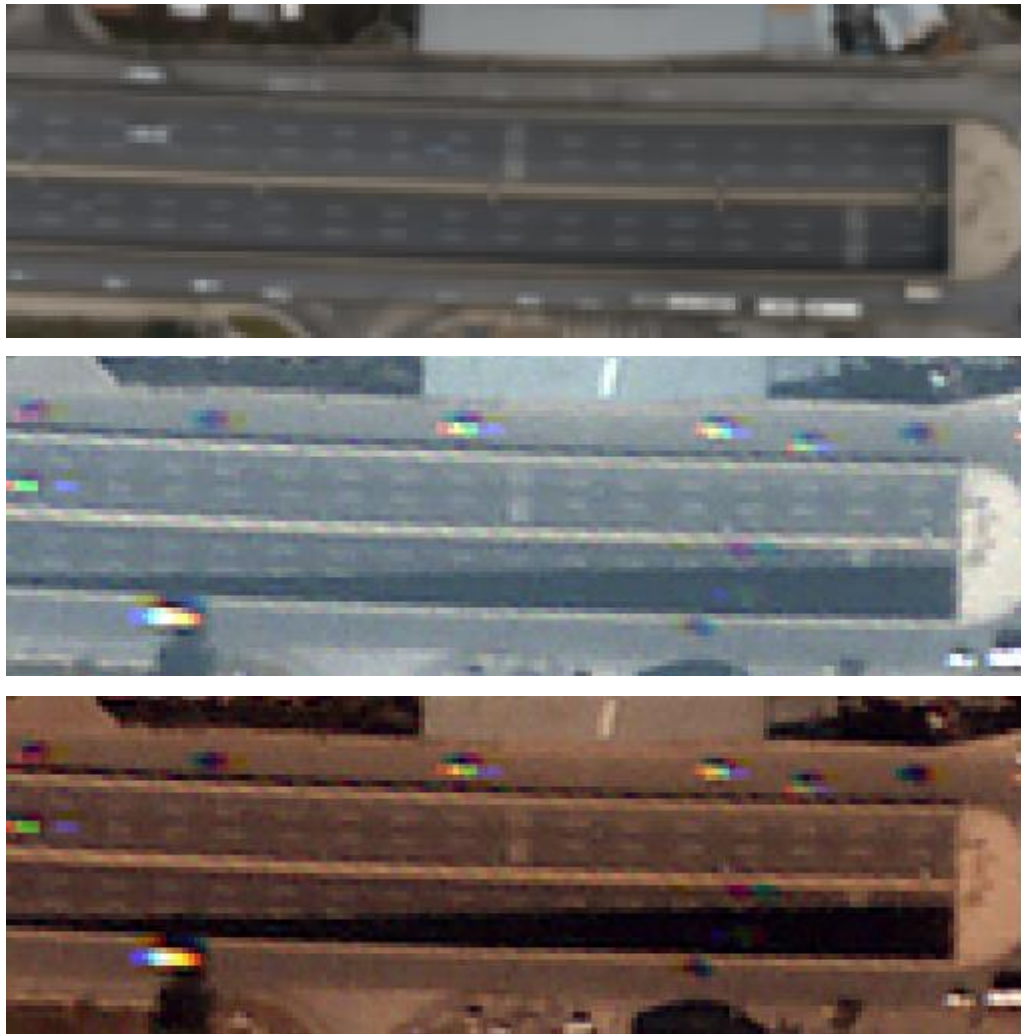
Apart from the moving objects, the colour artefacts may be sourced from large band-to-band registration errors. This issue can clearly be seen in Figure 4-3, Figure 4-7 and Figure 4-8.

The level of details in the UAV data and the SN30 images are in general equivalent as can be observed in Figure 4-1 to Figure 4-4. However, it can be seen in Figure 4.5 that the resolution may deteriorate depending on image part (blurring observed). Thus, the resolution varies within an image.

Although the GSDs of the Maxar and Pleiades images are different, the level of details visible in the images are similar as can be seen from road centre lines (Figure 4.6) and railways (Figure 4-7). Figure 4.8 shows that relief effect was also removed from the SN30 image, thus the image product is resampled for this purpose. It must be noted that the building located in Figure 4.8 is close to the edge of the image strip (ca. 450 m). Colour artefacts are visible also in this figure.

Although the overall image quality is good, aliasing is also observed frequently (see Figure 4-1 to Figure 4-3). Further examples to aliasing and colour artefacts in SN30 L3 image over Ankara are given in Figure 4-9.

The L1 and L3 images have different appearances due to the additional processing of the Red band. The histograms of SN30 L1 and L3 images over open terrain in Ankara are shown in Figure 4-10. There is a clear shift in the histogram of Red band.



20 m

Figure 4-1: Comparisons with the UAV orthophoto over a road with centre lines visible in: Top: UAV orthophoto; Middle: SN30 L1 image; Bottom: SN30 L3 image.

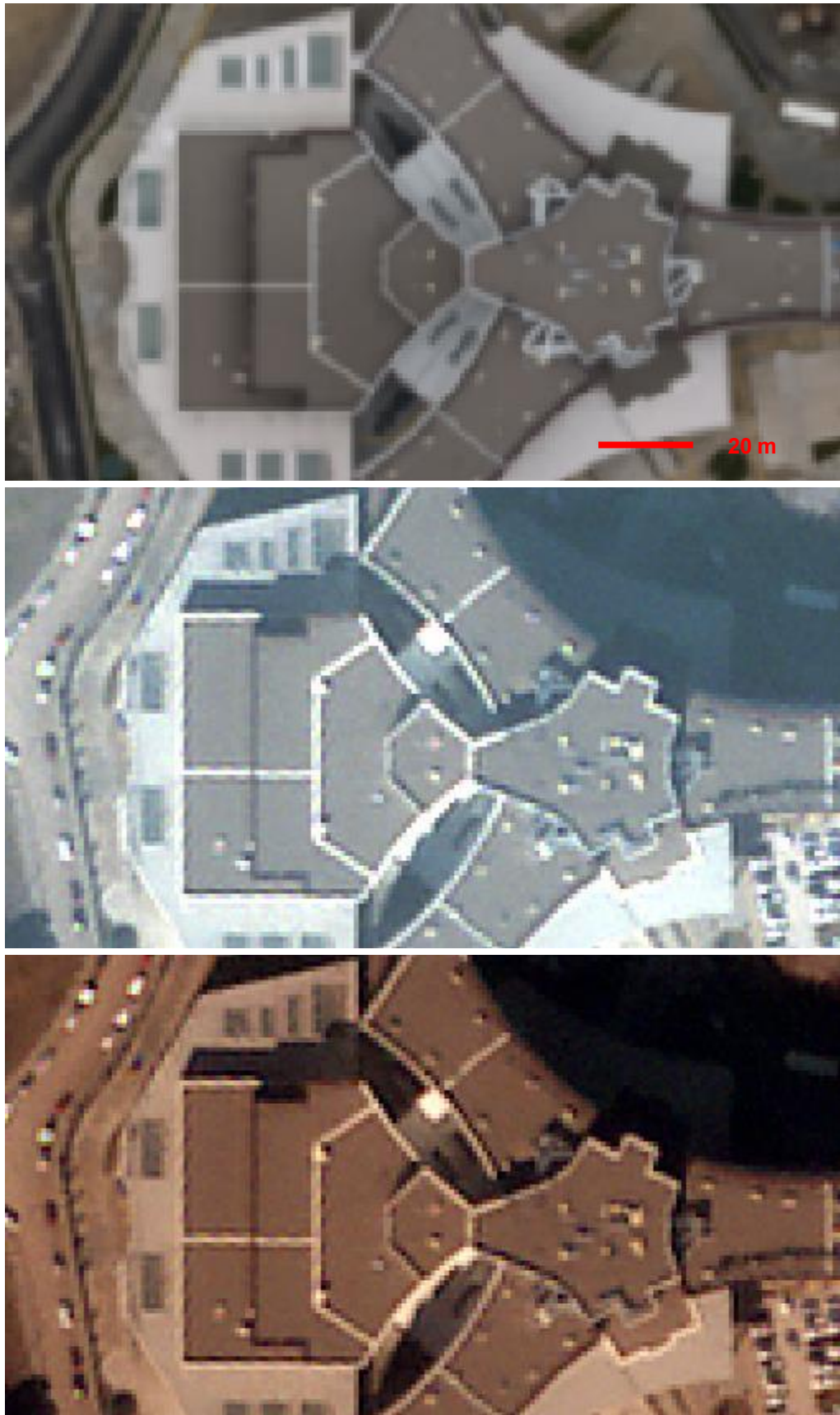


Figure 4-2: Comparisons with the UAV orthophoto over a building rooftop visible in: Top: UAV orthophoto; Middle: SN30 L1 image; Bottom: SN30 L3 image.

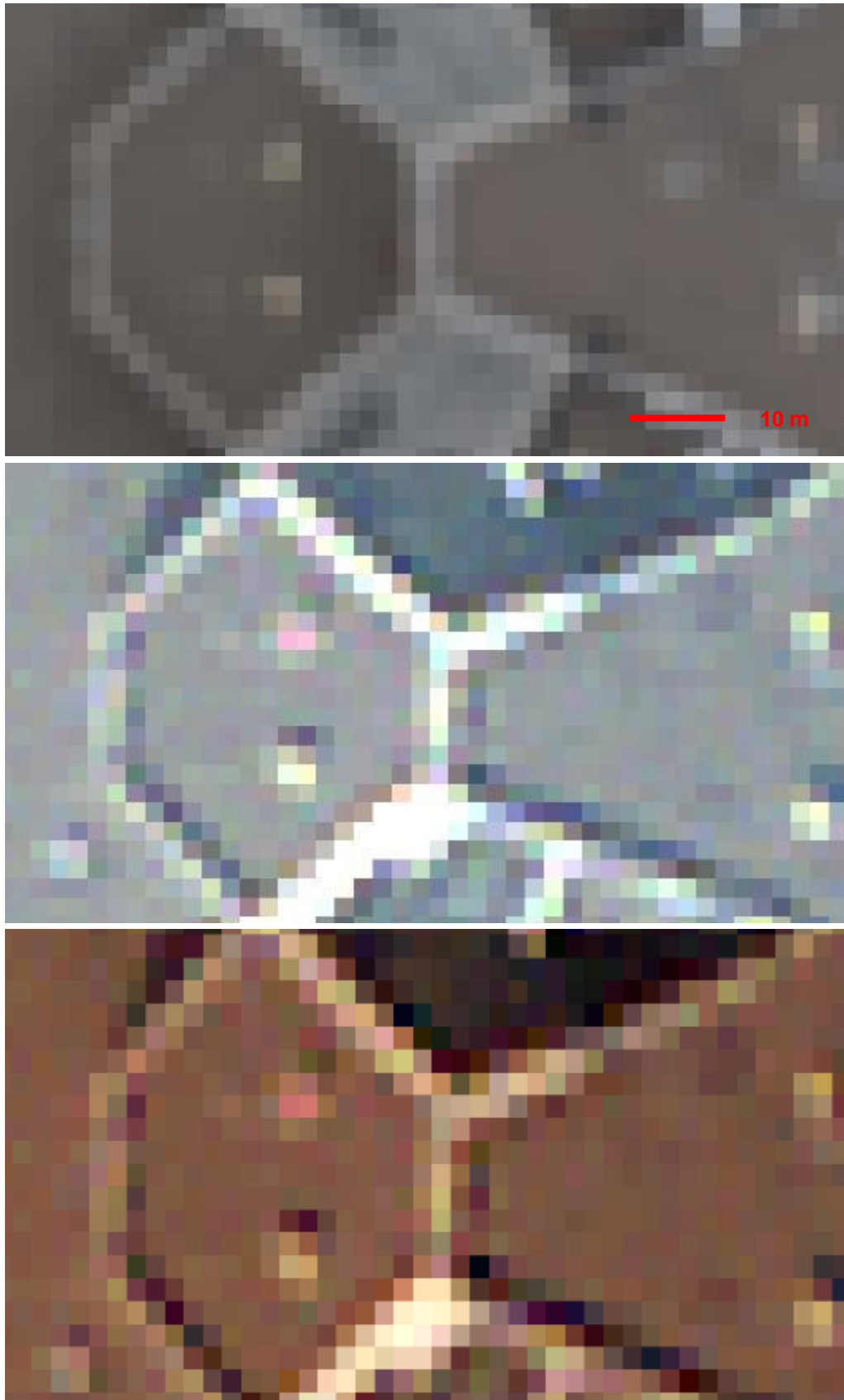


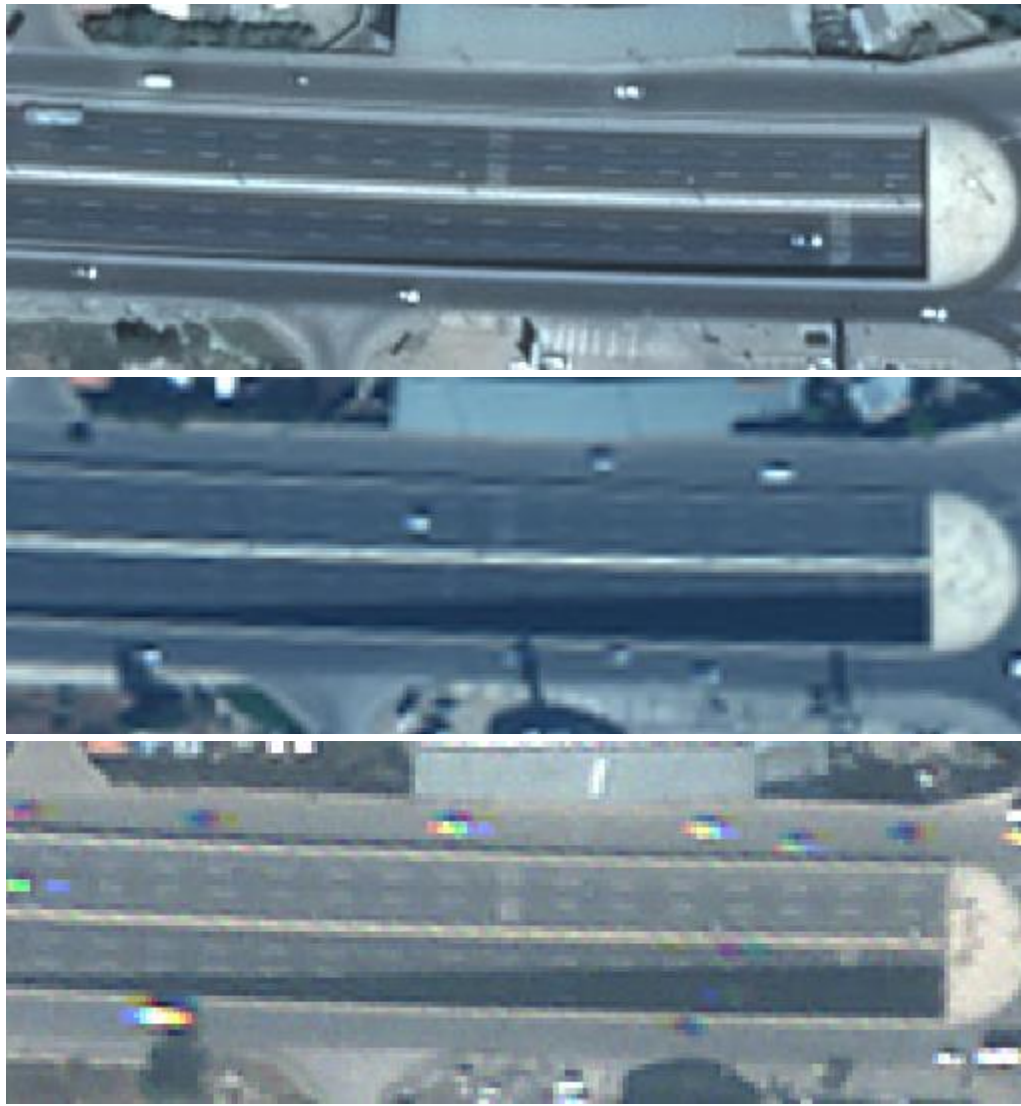
Figure 4-3: Comparisons with the UAV orthophoto over a building rooftop visible in: Top: UAV orthophoto; Middle: SN30 L1 image; Bottom: SN30 L3 image.



Figure 4-4: Comparisons with the UAV orthophoto over railways visible in: Top: UAV orthophoto; Middle: SN30 L1 image; Bottom: SN30 L3 image.



Figure 4-5: Comparisons with the UAV orthophoto over a soccer field visible in:  
Top: UAV orthophoto (1 m); Middle: SN30 L1 image (1 m); Bottom: SN30 L3 image  
(1 m).



20 m

Figure 4-6: Comparisons with the Maxar (13.10.2020, 60 cm multispectral ortho, and Pleiades (12.05.2021, 50 cm pan-sharpened ortho) data over Ankara test site. Road centre lines visible in: Top: Pleiades; Middle: Maxar; Bottom: SN30 L1 images.



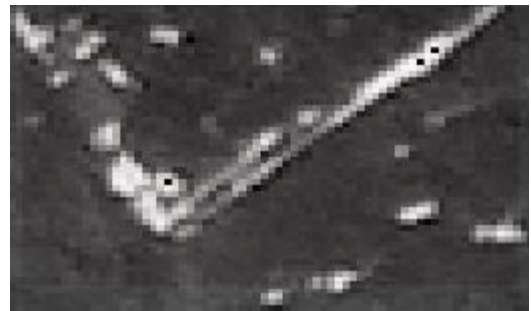
**Figure 4-7: Comparisons with the Maxar (13.10.2020, 60 cm multispectral ortho, and Pleiades (12.05.2021, 50 cm pan-sharpened ortho) data over Ankara test site. Railways and park visible in: Top: Pleiades; Middle: Maxar; Bottom: SN30 L1 images.**



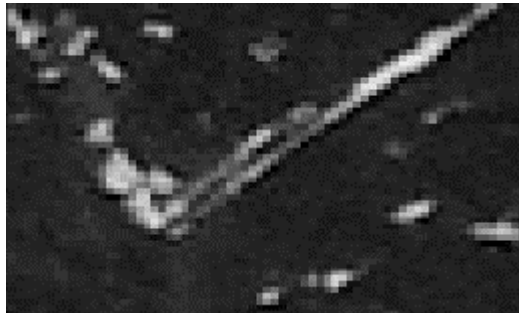
Figure 4-8: Comparisons with the Maxar (13.10.2020, 60 cm multispectral ortho, and Pleiades (12.05.2021, 50 cm pan-sharpened ortho) data over Ankara test site. Building rooftop visible in: Top: Pleiades; Middle: Maxar; Bottom: SN30 L1 images



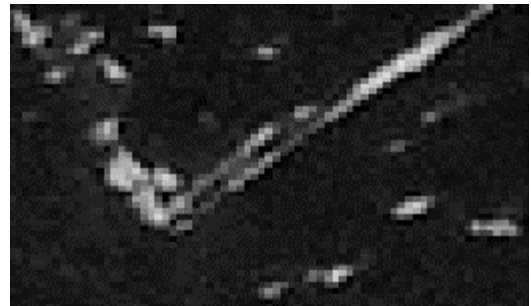
L3 MS



Red



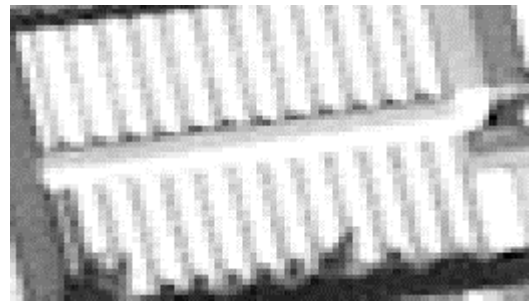
Green



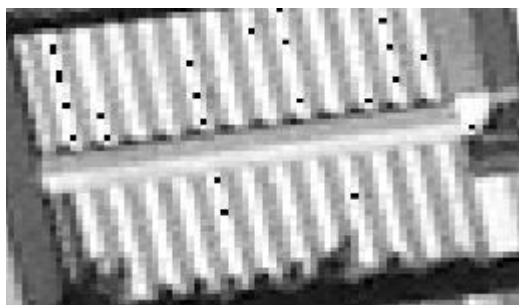
Blue



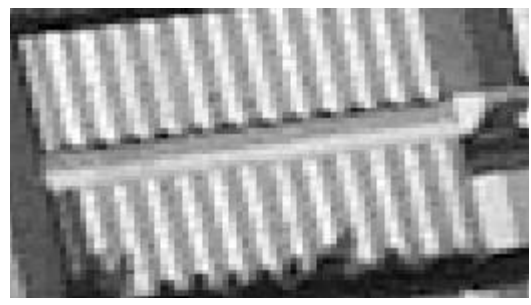
L3 MS



Red



Green



Blue

**Figure 4-9: Examples to colour artefacts such as aliasing and black pixels (not visible in L1 image).**



— 20 m

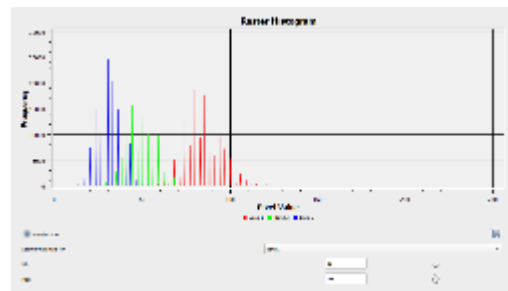
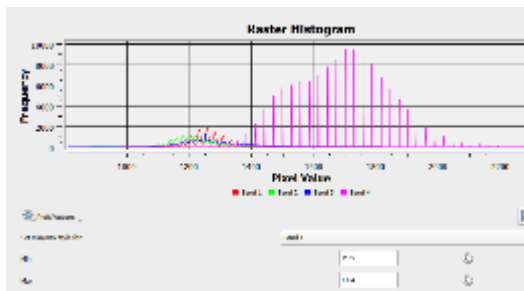


Figure 4-10: Histograms of SN30 L1 (left) and L3 (right) images over open terrain in Ankara.

### 4.3 Modulation Transfer Function (MTF)

The spatial resolution of a sensor has traditionally been a difficult concept to define, but all would agree that it is inextricably linked to the GSD and Instantaneous Field of View (IFOV) of an imaging sensor system.

As a measure of the geospatial quality of imagery, the MTF of the system is often used along with the SNR. The MTF is often used as a measure of image sharpness. This important parameter for image quality has to be checked on each orbit in order to be sure that launch vibrations, transition from air to vacuum, or thermal state have not degraded the sharpness of the images [RD-13].

#### 4.3.1 Method

The slant-edge method presented herein has been developed and operated in the context of the ESA contribution to the ALOS PRISM calibration campaign [RD-19]. The different steps of the algorithm are depicted within Figure 4-11 below and discussed thereafter.

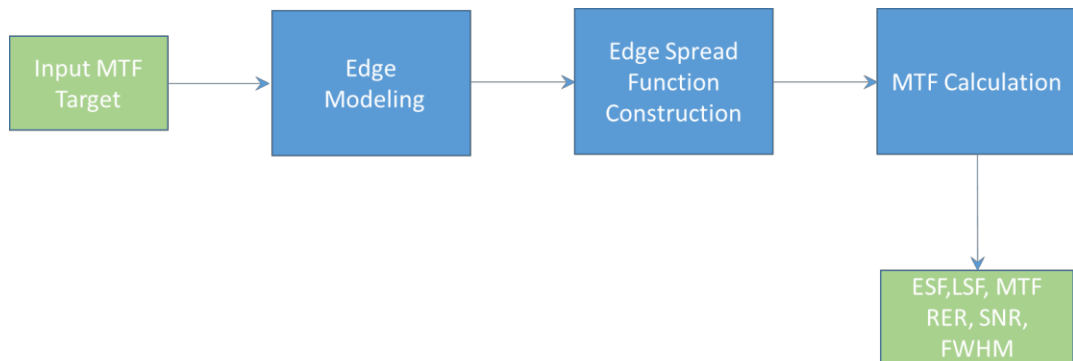


**Figure 4-11: Slant-edge method – algorithm steps.**

The input MTF target is a chequerboard image observed in all spectral bands. An image of the target, observed with NewSat (NS) is shown in Figure 4-12. The region of interest includes edge transitions, and nearly-vertical / nearly-horizontal edges are used to estimate MTF in the Along-track (AT) / Across-track (AC) direction or axis.

The method estimates, for any spectral channels, the MTF associated with the complete system response. The MTF is derived from computation of the Edge Spread Function (ESF) and Line Spread Function (LSF). These curves are accompanied with quality indicator metrics, such as Relative Edge Response (RER), SNR and Full Width at Half Maximum (FWHM).

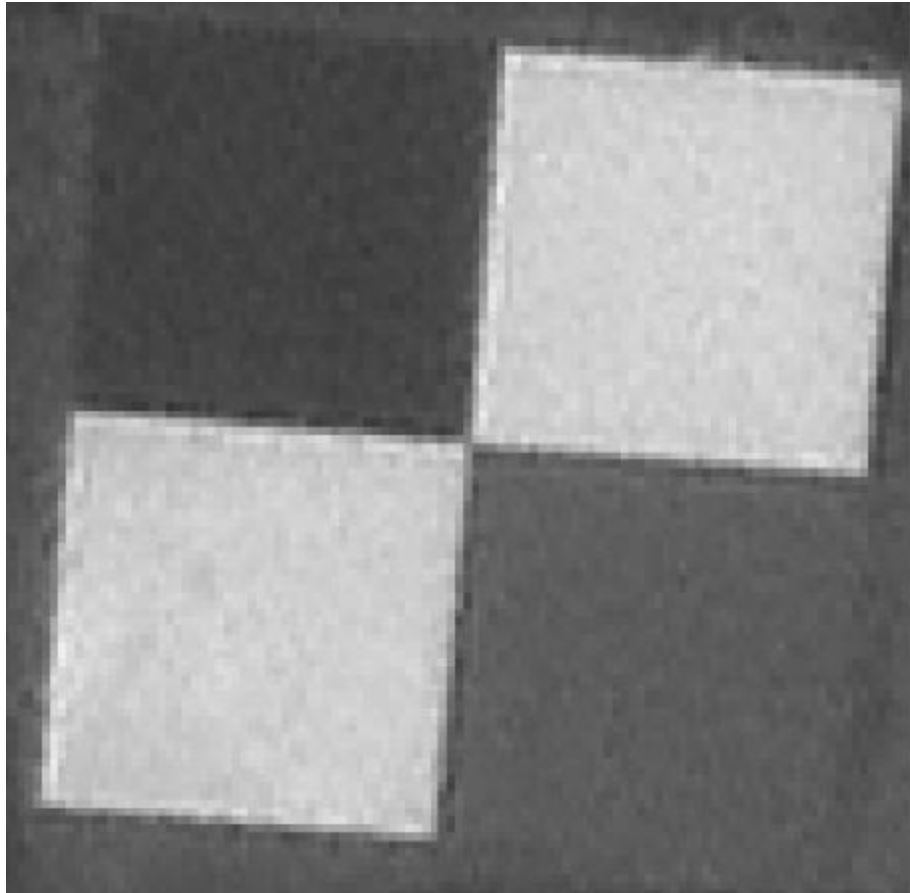


Figure 4-12: NS30 zoomed image (Blue channel) of Baotou MTF Artificial Target:

### Edge Modelling

The true MTF is defined normal to the edge. If the edge is slanted, MTF is calculated from the average of many sampling phases.

The construction of the ESF is inspired from [RD-14] where sampling phases are collected for a given orientation of the target. The Edge Modelling step is the estimation of the orientation of the target. As shown in Figure 4-13, for each image row included in the region depicted with rectangular form (Upper Left image), a parametric function is fitted in order to estimate the sub pixel location of the inflection point. Based on the set of inflection point sub pixel locations found, a least square method is used to estimate an overall orientation angle (Upper right image): the rotation angle. The per-row interpolated edge functions (Lower Left image) are checked and discarded in case of noise.

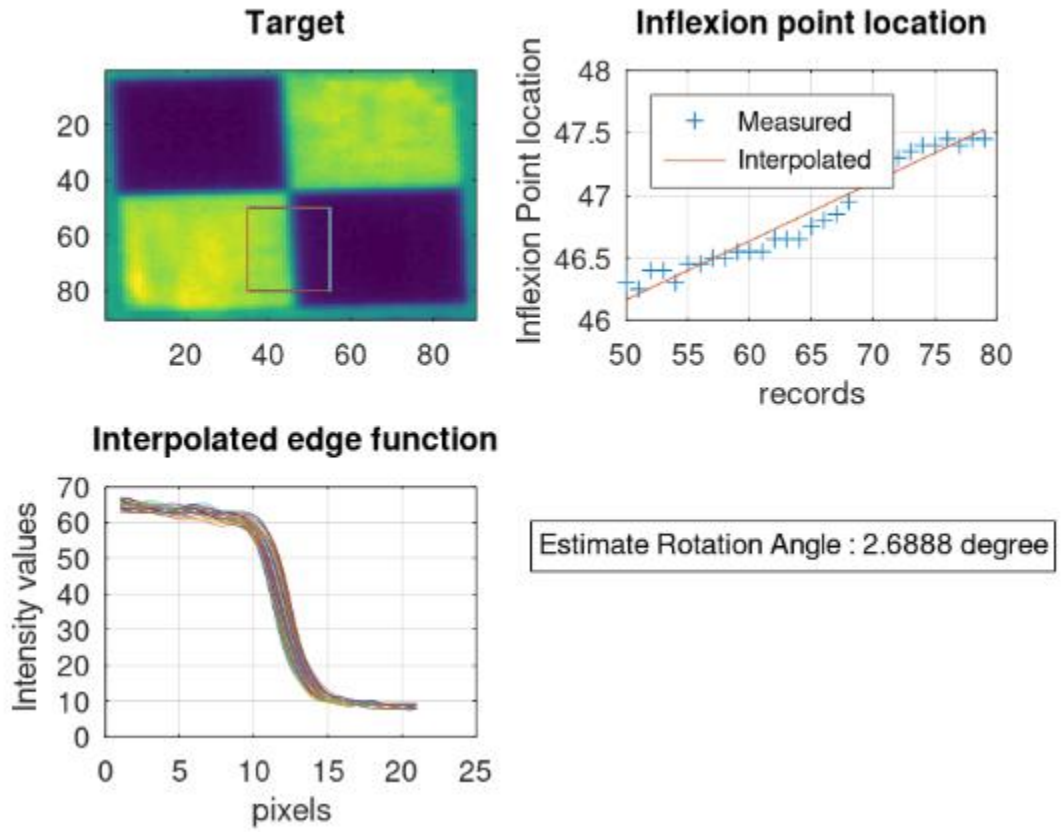


Figure 4-13: Slant-edge method – edge modelling output (NIR band).

In case of NS image, in some cases, there are issues to estimate inflexion point location due to inconsistent pixels (aliasing). For this reason, only a subsample of image lines is involved in the orientation angle estimate, as shown in Figure 4-14 below.

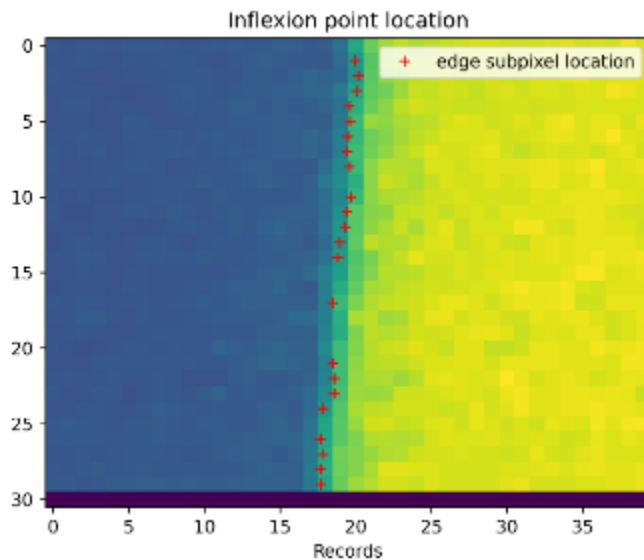


Figure 4-14: Determination of edge inflexion point location.

## Edge Spread Function Construction

The MTF method is very sensitive to noise and the orientation of edge should be accurately known. As mentioned before, a single image row is not sufficient to capture the various pixel phases accounting for aliasing and phase effects etc. The super-resolved target image is built applying the same approach for each image row and following these stages:

- Projection of each image pixel onto a line perpendicular to edge applying rotation angle estimated in the previous step, the method proposed by Kohm [RD-14] is used;
- Resampling of the pixel position in the new projection system, within bin of  $\frac{1}{4}$  pixel width.

Figure 4-15 shows the super-resolved target image with edge transitions that are now perfectly aligned. Depending on the expected direction (Along / Across axis), it is possible to define for each bin, the intensity value (pixel phase) of the ESF. By nature, in the final ESF, some bins can be left empty or include very few measurements causing noise. For this reason, the orientation angle should be carefully selected.

As some bins are definitely left empty, at this stage, the ESF data points are not uniformly distributed (not equally spaced). The Locally Estimated Scatterplot Smoothing (**LOESS**) curve fitting algorithm (locally weighted non-parametric regression fitting using a 2nd order polynomial) is used to resample the data to uniformly spaced sample points.

It is worth noting that the process does not fit a parametric model (sigmoid for instance) to the data points, the proposed approach herein is a non-parametric approach. More noise will be captured and results are closer to the system behaviours.

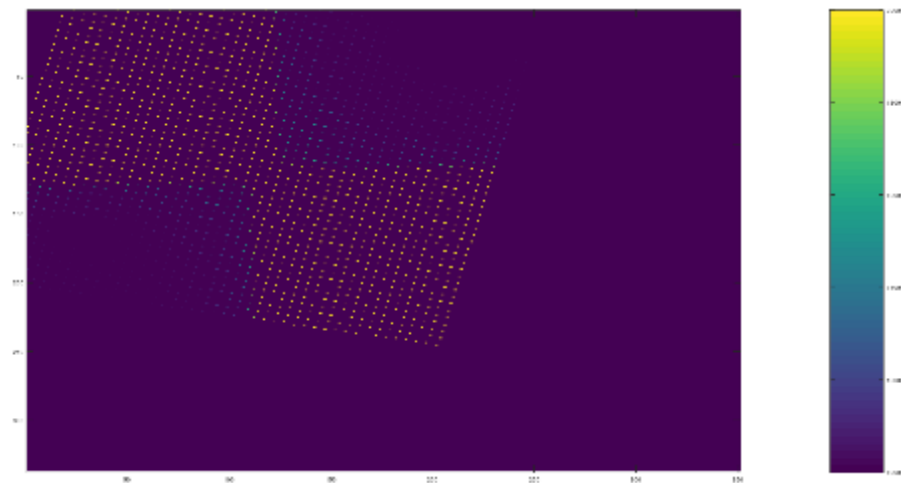


Figure 4-15: Super Resolve Target (0.25-pixel bin).

## MTF Calculation

The final stage is to compute MTF by using a derivative method: computing the finite difference approximation of the uniformly spaced ESF to produce the LSF.

The LSF may contain high frequency noise, amplified by the derivative method. A local smoothing with fourth order Savitsky Golay filtering is applied (window size is 11 bins) to remove outliers. At the end, a Hann window is applied to the ESF (three-term weighted average smoothing technique) and a smooth LSF is obtained.

The main outputs of the method are shown in Figure 4-16 below and can be summarised as follows:

- The ESF – top left graphic,
- The LSF or ESF derivative – bottom left graphic,
- The MTF as LSF expressed in the Fourier domain – upper right graphic,
- The LSF together with LEOSS interpolated LSF, allowing to check intensity estimated for all empty bins – lower right graphic.

It is worth noting that in the ESF plot, variations located in the upper part of the curves are observed and these might be attributed to noise over uniform bright parts of the chequerboard. These variations are seen in the LSF plot, located in the right part outside the peak. The derivative filter is very sensitive to the noise, and therefore noise, is impacted strongly by the quality of measurement. These variations are seen in data from other HR EO missions and are mainly due to the quality of the chequerboard target.

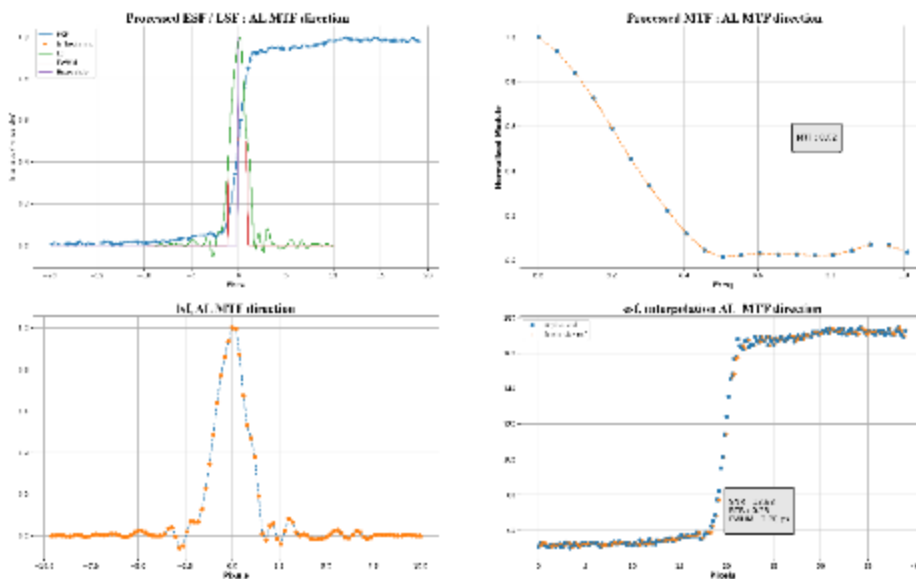


Figure 4-16: Standard outputs of the MTF processing.

### 4.3.2 Data

The selected ROIs for MTF artificial targets are Salon-de-Provence Airport, (France) and Baotou calibration site (China). At the end of 2022, the MTF target based in France has been cleaned and partially repainted, as shown in Figure 4-17.

The MTF assessment considers as input edge image. An aCross Track (**CT**) edge image is used to estimate Along Track (**AT**) MTF. Conversely, an AT edge image is used to estimate CT MTF. Considering this latter statement, Salon target is relevant to assess CT MTF.

The MTF TDS included five products (two from Salon and three from Baotou), as detailed in APPENDIX B.

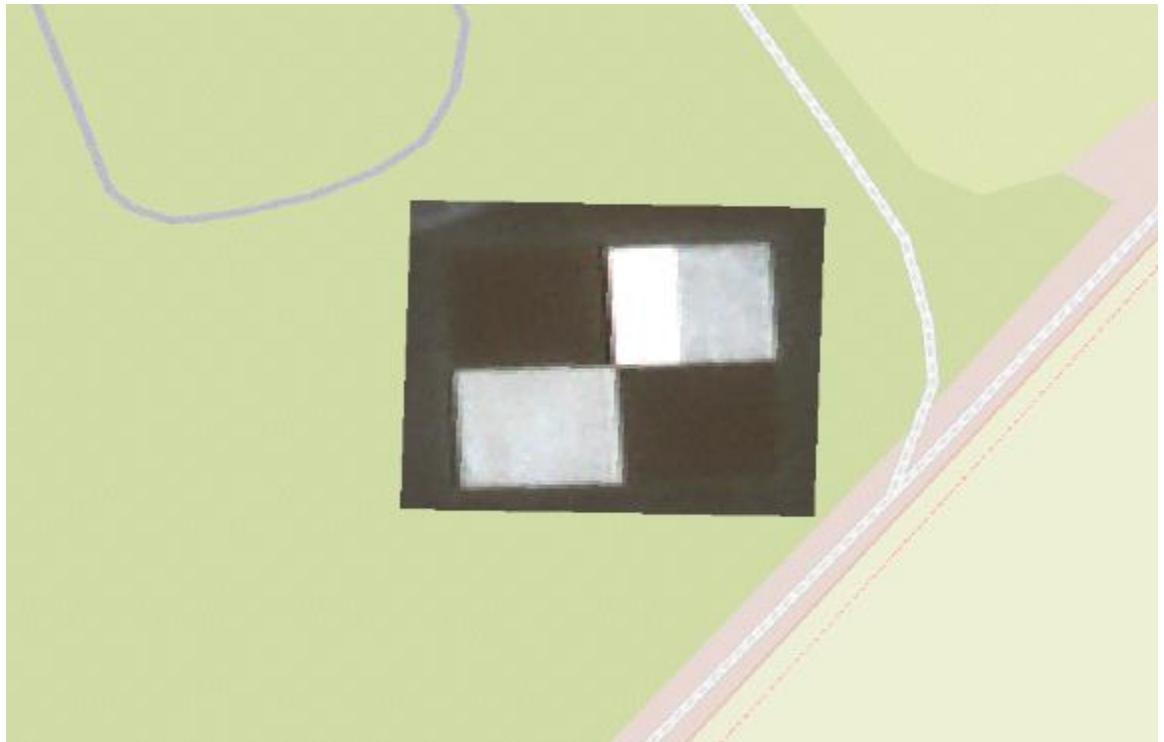


Figure 4-17: NS Image of Salon Target and nice AT edge.

### 4.3.3 Results

As shown in Table 4-1, Table 4-2, the AT/AC MTF are mostly within specification (0.1 @Nyquist) in particular for CT MTF. The results are varying a lot depending on NS satellite and processing version. The CT MTF results from Salon images are good, whilst for some Baotou images; 20220618\_062155\_SN30, 20220614\_\_041502\_SN29 accuracy results are outside specification. For those before mentioned products, the processing baseline is the s/w version '0\_50' and it might be a cause. Also, CT results estimated based on these products have been removed from the TDS. MTF results obtained from product process with s/w 0\_52 are more consistent.

The L1 images are results of many processing chains including contrast restoration and anti-aliasing. In some cases, the resulting reconstructed ESF profile is correct / nominal and in some other cases ESF profile displays inconsistent edge artefacts ("halo").

In the nominal case, the contrast enhancement is visible in the MTF shape, high MTF values before Nyquist frequency, close to 0 value after Nyquist frequency, as shown in Figure 4-18 and the edge artefact does not affect image quality.

In some cases, as shown in Figure 4-19, the sharpening seems to be stronger, and contrast not correctly enhanced, resulting in a lower MTF value.

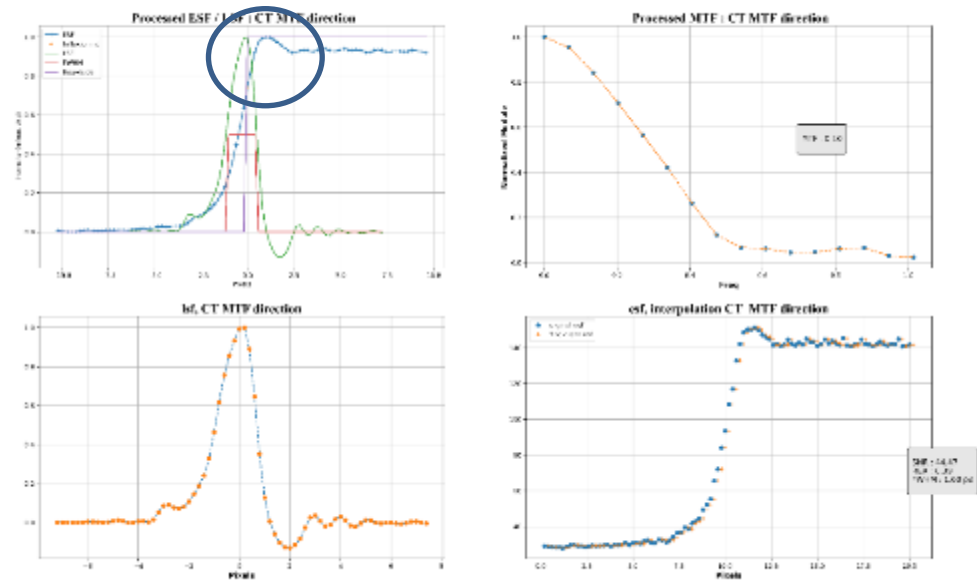


Figure 4-18: SN30 Lacrau Image, BD3 MTF Results and edge artefact (“halo”).

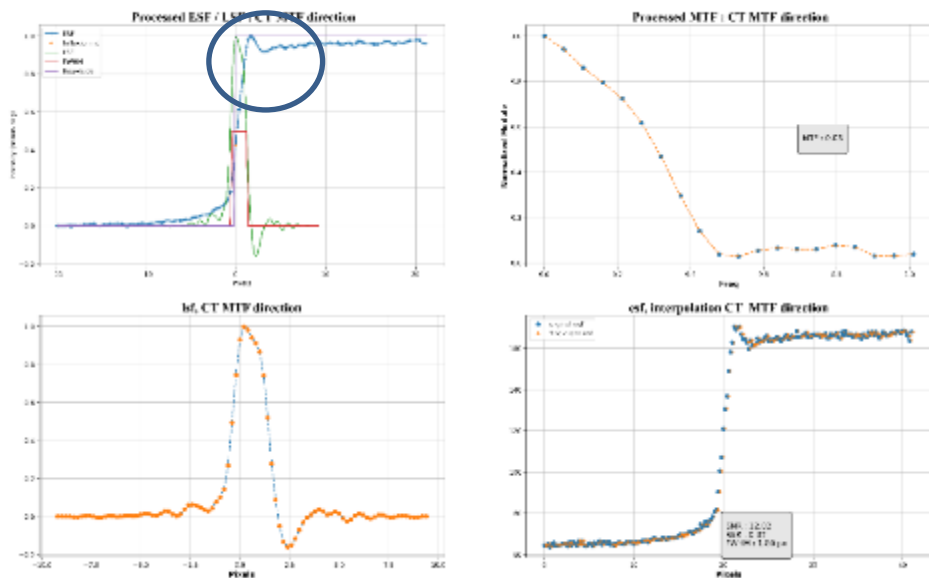


Figure 4-19: SN30 Baotou Image, BD3 MTF Results and edge artefact (“halo”).

Overall AT/CT results are listed respectively in Table 4-1, Table 4-2, for each indicator (RER, FWHM, MTF@Nyq), mean and standard deviation values over working sample is indicated. Note that the proposed EDAP method is non-parametric, and therefore is sensitive to noise, it explains, to some extent, the varying results.

The CT results (RER; FWHM; MTF) are in all cases better than the AT results which is common because of motion blur. In addition, results are consistent across images from

Blue, Green and Red channels but the AT / CT results of image from the NIR channel are below.

**Table 4-1: Along Track (AT) MTF Results**

	RER		FWHM (m)		MTF@Nyq.	
	Mean	Std	Mean	Std	Mean	Std
Channel 1 (Blue)	0.42	0.08	1.33	0.12	0.08	0.04
Channel 2 (Green)	0.46	0.05	1.67	0.12	0.11	0.09
Channel 3 (Red)	0.40	0.09	1.80	0.35	0.06	0.07
Channel 4 (NIR)	0.36	0.06	1.93	0.12	0.03	0.01

**Table 4-2: Cross Track (CT) MTF Results**

	RER		FWHM (m)		MTF@Nyq.	
	Mean	Std	Mean	Std	Mean	Std
Channel 1 (Blue)	0.47	0.10	1.53	0.31	0.14	0.08
Channel 2 (Green)	0.47	0.12	1.67	0.12	0.13	0.01
Channel 3 (Red)	0.45	0.08	1.60	0.20	0.13	0.08
Channel 4 (NIR)	0.34	0.05	1.53	0.31	0.10	0.04

## 4.4 Signal To Noise Ratio (SNR)

The SNR is an important image quality indicator. Visual interpretation of an image does not require high SNR data: even in the presence of noise, an operator is able to identify objects. However, multispectral image processing requires high SNR values in order to control uncertainties in the measurement as much as possible.

For each band, the SNR value and its corresponding average reference radiance  $W. sr^{-1}m^{-2}$  are given. The proposed method herein has already been implemented in the context of other EDAP assessments. A description of the method is provided below.

### 4.4.1 Method

The SNR is a measure of the mean signal to noise ratio. In the scientific community, there are two types of SNR typically measured; the temporal SNR and the spatial SNR. The basic formulation of the SNR is given by:

$$SNR = \frac{\mu}{\sigma}$$

Where:

- $\mu$  is the mean signal,
- $\sigma$  is the standard deviation of the signal.

The herein proposed method estimates the spatial SNR considering the statistical distribution over a set of “small windows” (5 pixels by 5 pixels), whereby referring to the previous mathematical relationship:

- The “mean signal” is defined as the spatial average of a group of pixels in the “small window”;
- Noise is typically defined as the standard deviation of a region of pixels in the “small window”.

Each spectral band image (radiance measurement) is processed with the modified algorithm initially proposed in [RD-12]. The algorithm has been modified to allow the selection of small windows of uniform image intensity (condition 1), and the selection of small windows mostly located over regions with a flat terrain relief (condition 2).

For conducting this SNR assessment, a uniform / bright scene has been selected. The existing Libya-4 dataset, usually involved in the inter calibration exercise, appears to be appropriate for this purpose. The site uniformity increases over small areas, and this is the reason for which small windows are selected. However, the spatial high frequency image content still exists, specifically at locations of sharp transitions (e.g., desert dune summit). To overcome this issue, a dedicated image processing is applied to detect high frequency content and filter small windows (image window processing with Sobel operator).

Also, the different steps of EDAP SNR algorithm are summarised as follows:

- Create SNR image, considering as input, image converted to radiance measurements, and iterating on “small windows” to compute SNR;
- Compute local statistics over 5 pixels x 5 pixels sliding window on the terrain relief data and the image edge response (Sobel Operator);
- Select the set of “small windows” displaying uniform content and located in flat areas;
- Compute the statistical distribution (histogram) of “small windows”  $\frac{\mu}{\sigma}$ ;
- Location of the peak in the histogram of SNR image is a measure of the system SNR;

- Report the SNR value at the peak and the corresponding mean radiance value;
- Control SNR distribution based on report including several graphical representations as shown in the Figure 4-20.

This report includes the following graphics:

- The top left graphic used to check that pixel selection is consistent; and one can expect a Gaussian distribution of values within each bin of radiance values.
- The bottom left graphic is used to appreciate how SNR is changing against bin of radiance values, one can expect very limited evolution within the considered radiance interval.
- The top right graphic is the histogram of selected pixel values.
- The bottom right graphic is the histogram of the SNR image.

The top left graphic is based on the image of difference (**DIFF**) defined as the difference between input image and input image with uniform filtering applied. Also, the DIFF image exhibits high frequency content. When removing from DIFF image, signal due to edge, one can expect to get noise information.

The results show in the bottom right and in the bottom left graphics, both are dealing with SNR. More confidence can be attributed to the bottom right one, because more measurements are taken into account (in the bottom left graphic, it is only per bin). As mentioned before, we expect, within radiance interval, very small changes affecting the SNR curve (Blue, bottom left graphic) and finally a mean value of the same order as the value deduced from 'snr cumul' (Green, bottom right graphic), that is the location of the peak.

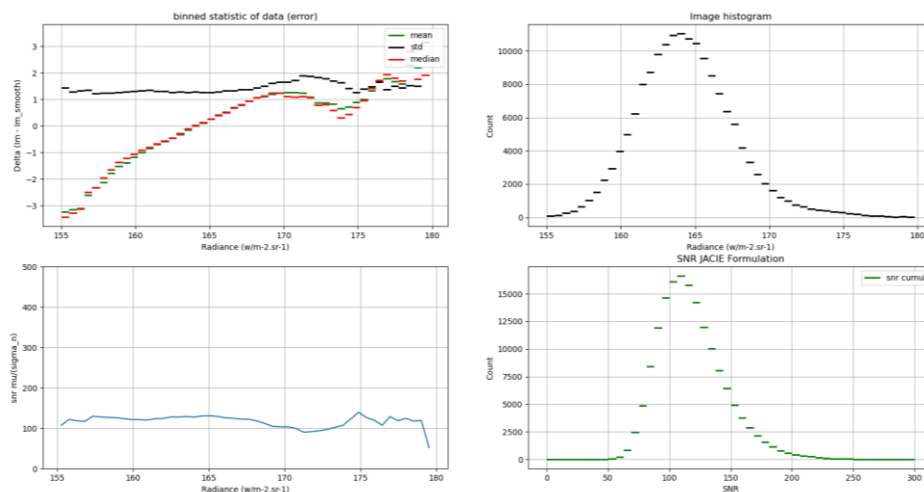


**Figure 4-20: Standard graphical outputs for SNR assessment.**

Input 16-bit images are scaled to radiance images and to Top Of Atmosphere (**TOA**) images by using coefficient included in the product metadata file. For validation purposes, scaling factors to convert digital number to radiance values have also been computed independently.

The SNR is a function of the mean radiance of the landscape. The SNR is usually lower for low value of radiance (dark landscape) because the relative influence of the noise is larger. For large radiances, the SNR increases as the relative influence of the noise decreases.

We are working herein with a bright site; the SNR is expected to be high for most bands. As shown previously, the considered radiance intervals are quite small and do not allow to observe variations. Based on only one uniform test site, a noise model cannot be estimated.

The input product level is Level 1, and EDAP did not apply additional geometric processing to express data within the instrument grid. As a result, column-wise noise and line-wise noise cannot be assessed separately.

#### 4.4.2 Data

The Region Of Interest (**ROI**) is within the Libya 4 site, and is defined within the full image extent. The background values are discarded from the selection, and this region is common to three products observed over Libya 4 (as detailed in APPENDIX B). The size of window is 1000 pixels x 1000 pixels. Two image windows are considered, both located at the following upper left coordinates (line / pixel) 4500 / 4500, 3500 / 3500.

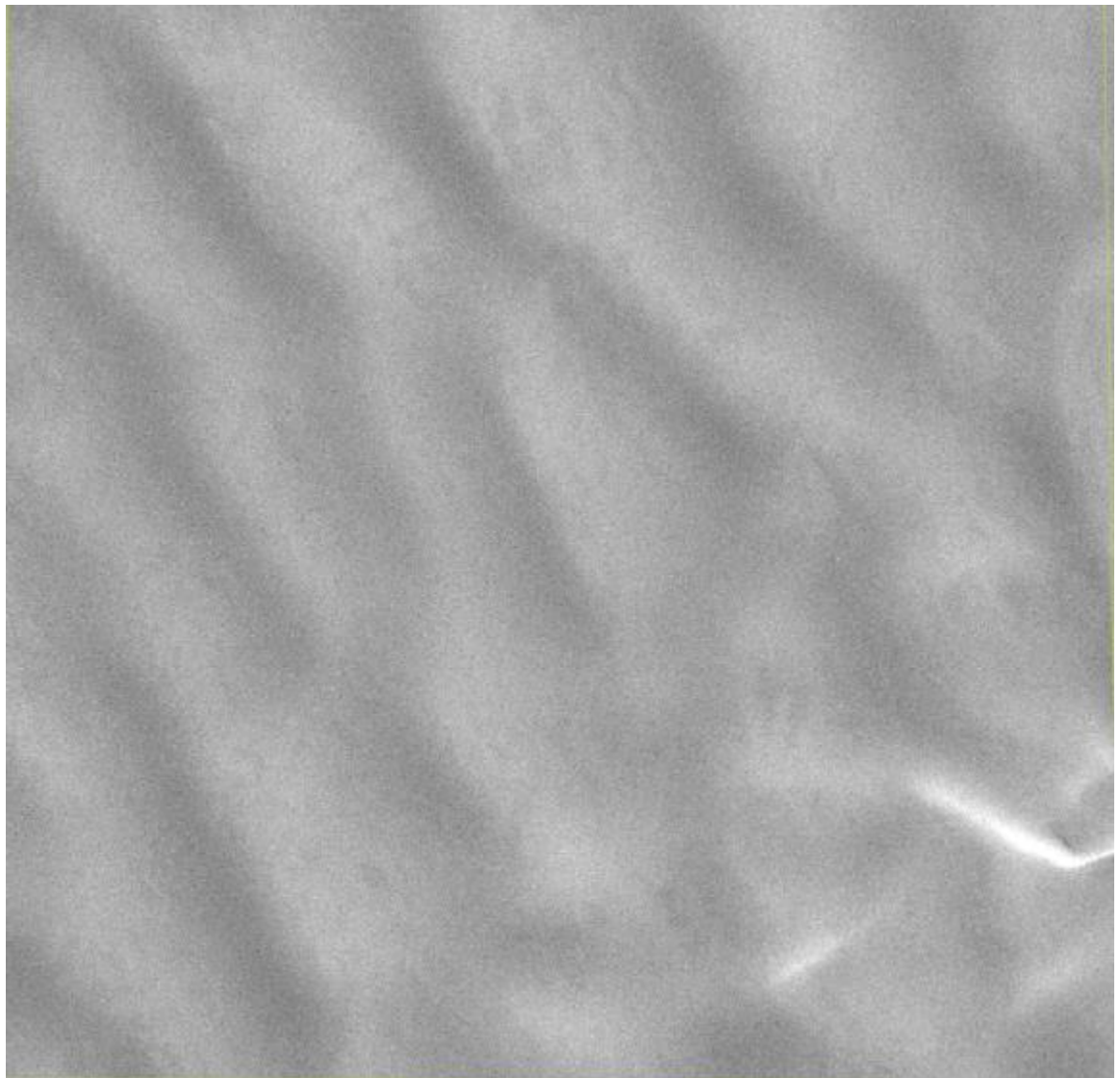


Figure 4-21: 20230109\_115258\_SN30\_L1\_MS\_0 – SNR ROI 1 - (Blue Band)

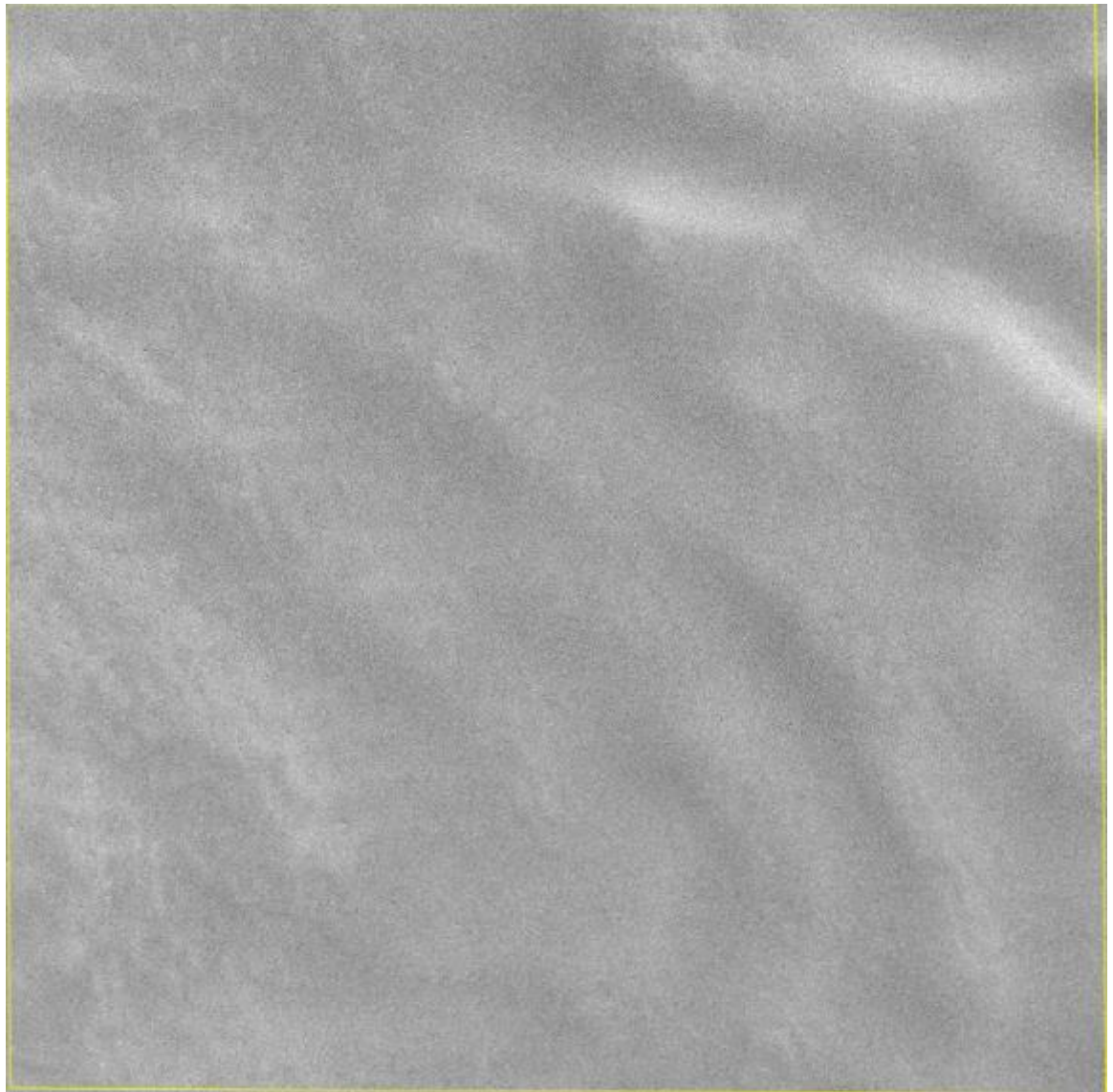


Figure 4-22: 20230109\_115258\_SN30\_L1\_MS\_0 – SNR ROI 2 - (Blue Band).

#### 4.4.3 Results

In Table 4-3, the *SNR* results are given against a reference radiance and a particular reference TOA reflectance.

The *SNR* statistics are computed by using three products / three observation dates and two ROIs. The results are listed in table below.

Table 4-3: SNR results

NS Spectral Bands	Mean $SNR(\rho)$	Std SNR	Reference RADIANCE	$\rho$ (TOA)	# observation dates
Blue	83.70	4.71	97.68	0.25	3
Green	82.32	5.48	115.00	0.31	3
Red	102.98	10.38	137.51	0.43	3
NIR	78.64	6.39	114.17	0.52	3

Due to the method, results might depend on the selected ROI. As shown in both Figure 4-23 and Figure 4-24 below, results from both ROIs are roughly equivalent. The Red band SNR results are better than the SNR results of the other bands. The SNR of NIR band is a bit lower than the other bands, as also observed within visual inspection activities.

Based on these results, at a first glance, there is no difference between SN27 / SN30 results considering our uncertainty level. Looking in more detail at Figure 4-23, results of the two products dated of the same day (20230109) differ and show improved SNR for SN30 data (might be due to satellite lifetime difference).

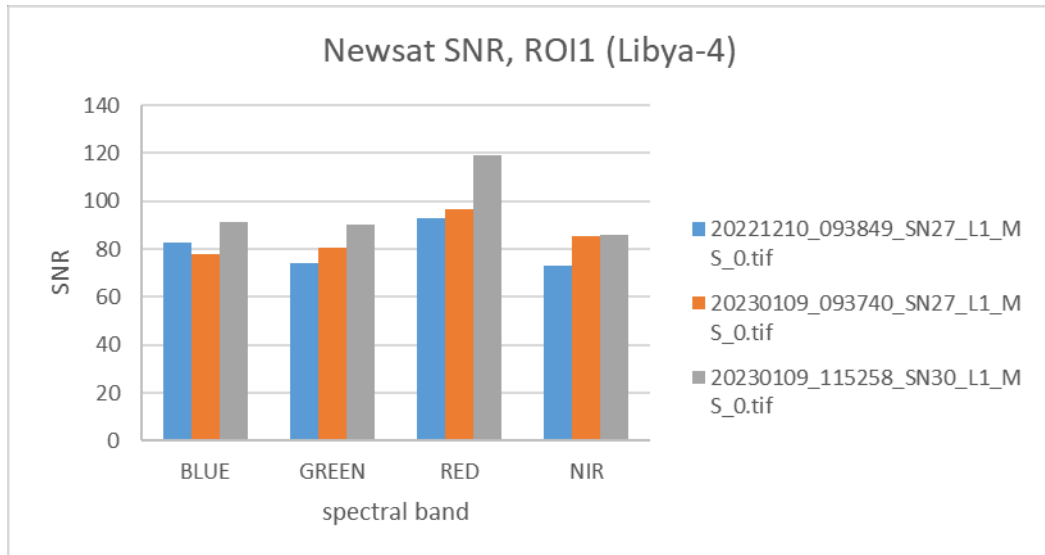


Figure 4-23: Mean SNR of each band for the three products (ROI1).

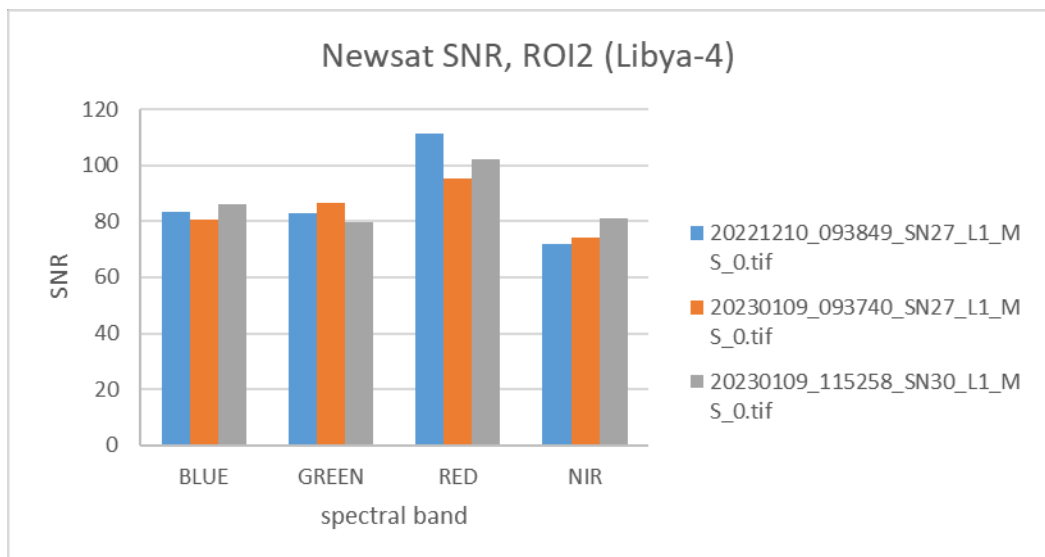
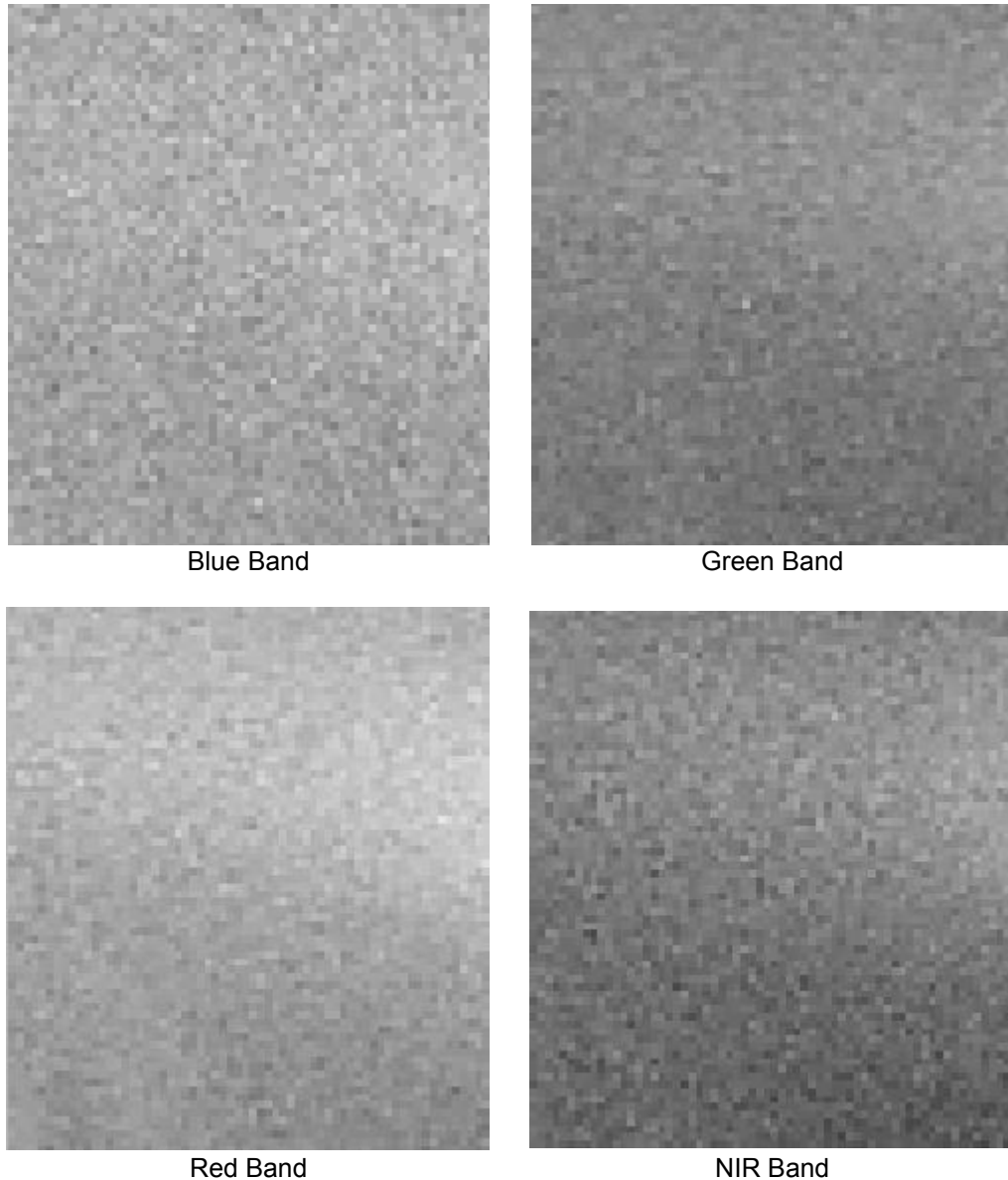


Figure 4-24: Mean SNR of each band for the three products (ROI2).

Figure 4-25 shows the full resolution image window for every band (line / pixel of upper left coordinate in the full image is about 3600 / 4000.). Less noise is visible in the Red band which looks smooth compared to the other ones (Blue, Green NIR bands).



**Figure 4-25: Full resolution image windows (Libya 4 data).**

The SNR images as shown below highlight some abrupt SNR changes at several image row locations. These image row locations are changing depending on spectral band. Moreover, these are changing depending on observation date. Regarding the root causes, these are two folds and are summarised as follows:

- When changes arise in the image row direction, this is more likely due to equalization between image tiles.
- When changes arise along the oblique line, still in image row direction, this is more likely due to equalisation between image frames.

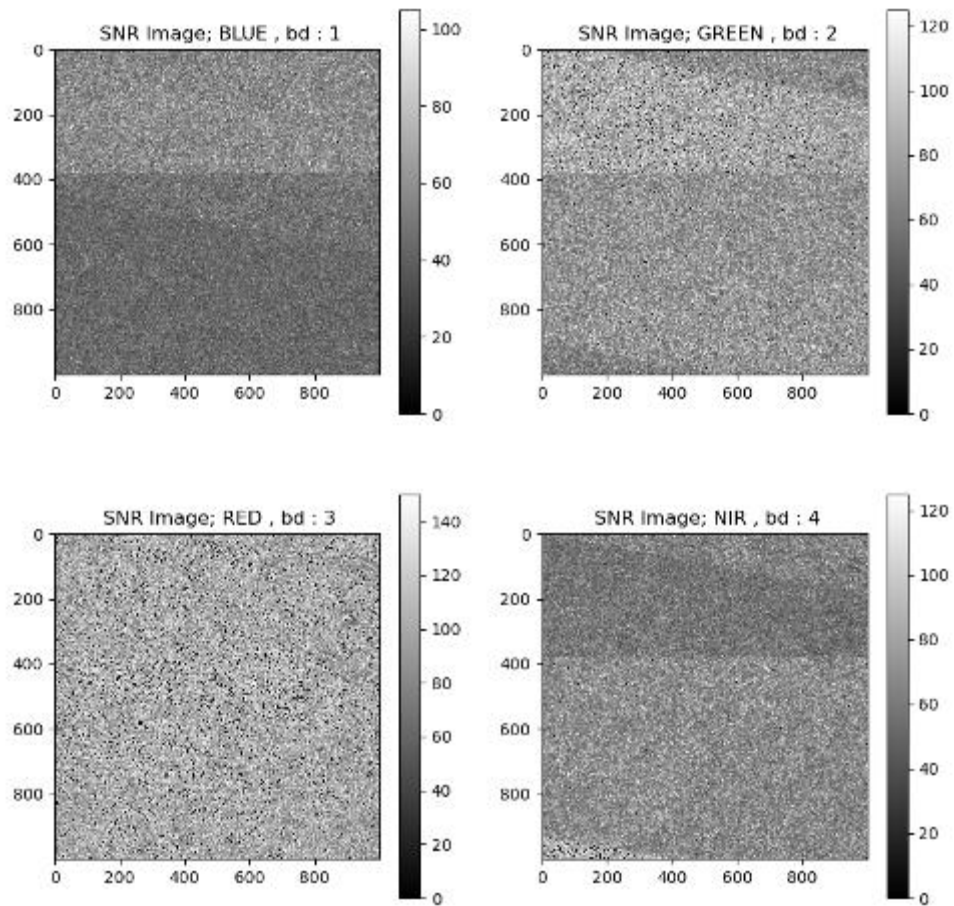


Figure 4-26: SNR Images (ROI 2).

## 4.5 Results Compliance

The Signal to Noise specification from the data provider is indicated to be “100 @  $\rho=0.5$ ” whatever the spectral bands. As shown with this validation exercise, the SNR of NS images is slightly below 100 (for reflectance lower than 0.5).

NS specifications are more likely related to the camera itself, without considering the noise of Level 1 / Level 3 processing itself. Taking into account the uncertainty of the EDAP method and the representativeness of the dataset, one can state the compliance of the NS product with the accuracy specification claimed by the data provider.

Regarding MTF, this preliminary study led to many observations as follows:

- Image quality of TDS is in general of varying quality depending on observation dates, processing baseline (s/w version)
- AT / CT MTF @Nyquist is around 0.1 for the last processing baseline which is in agreement with the specification claimed by the data provider
- AT MTF is degraded compared to CT MTF
- The processing baseline (s/w version) change affects CT MTF and does not affect AT MTF
- NIR Image quality is below Blue, Green, Red Image quality
- Overall results are in agreement with USGS ones.



- All these statements should be considered whilst taking into account the assessment method for which model is non-parametric, it can be seen as pessimistic, because it is very sensitive to any quality issues.

## 5. DETAILED VALIDATION – GEOMETRY

### 5.1 Introduction

This assessment proposes to validate the geometric specification of the NS Level 1 end-user product.

As Level 1B (L1B) products are not disclosed to the end user, this assessment does not address the geometry of the L1B product. Moreover, as there is no difference between Level 1 / Level 3 (L3) geometric grids, L1 product results are assumed to be similar to L3 ones.

In this context, the following geometric data quality aspects were addressed:

- Absolute georeferencing accuracy (planimetric only) obtained from Red Green Blue (**RGB**) images as is (no improvements with GCPs)
- Temporal accuracy (between two or more acquisitions of L1 product level)
- Multispectral Interband registration (between the multispectral bands of L1 Product, Green band taken as reference).

For the absolute accuracy validation items, the results were found in agreement with the accuracy specifications (<10 m CE90) given by the data provider in [RD-5] and the results (10.77 m CE90) given in the USGS System Characterization Report on the Satellogic NS Multispectral Sensor [RD-11]. No temporal accuracy specification or reporting exists. Therefore, we follow the absolute accuracy specifications for this purpose. The temporal accuracy results are in agreement with those given by the data provider.

Regarding the image inner accuracy, large variations were observed within an image. Although no specification or report exists on this aspect, the variations over mountainous topography exceed the global absolute accuracy. Quantization of this aspect was performed only by samples and not systematically. Yet, it can be said that the inner accuracy results do not comply with the absolute accuracy specifications over mountainous areas.

### 5.2 Absolute Geolocation Accuracy

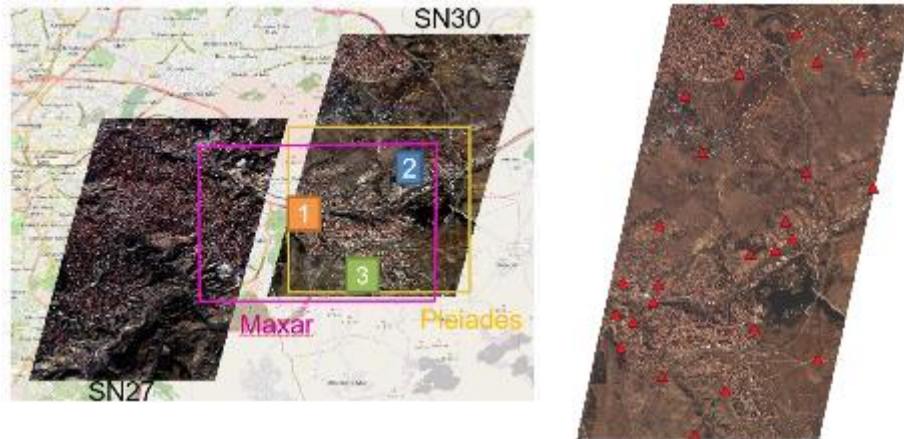
#### 5.2.1 Method

The methodology for the absolute geolocation accuracy assessment is based on an external reference, i.e., GCPs surveyed by using Global Navigation Satellite System (**GNSS**) instruments and UAV orthophotos with 3-5 cm GSD, over Ankara (Turkey) test site. A total of 25 GCPs were measured on the SN30 L1 data manually with an approximate measurement accuracy of half a pixel. A comparison of GCP coordinates between those measured on the orthorectified images and GNSS-surveyed ones with cm accuracy was performed in X and Y directions and evaluated by using statistical measures (i.e., mean, standard deviation and Root Mean Square Error (**RMSE**)).

In addition, an image2image comparison by using a dense image matching technique (KLT tracking) was applied between the reference UAV orthoimages and SN30 acquisition over Ankara. The KARIOS tool, [RD-9] was used for this purpose. The results were evaluated by statistical measurements and also visually.

## 5.2.2 Data

SN 27 image taken on 30.12.2022 and SN30 image taken on 22.02.2023 were used for the evaluations over the Ankara site (see Figure 5-1). Only SN30 image was assessed for the absolute accuracy using GNSS-surveyed GCPs and the UAV images as reference.



SN27 and SN30 image coverages over Ankara site shown on OpenStreetMap base map and the extents of UAV sites (numbered with 1,2,3) and the Maxar and Pleiades imagery used for visual inspection in section 4.2.

The distribution of GCPs over the SN30 L3 image.

**Figure 5-1: Reference equipment for absolute geolocation accuracy assessment.**

## 5.2.3 Results

The results of the 2D accuracy analysis based on 25 GCPs are presented in Table 5-1. The SN30 product from 22.02.2023 was evaluated. No systematic behaviour was observed in the distribution of discrepancy vectors (see Figure 5.2). The CE90 results (1.37 m) are below the CE90 specification (<10m).

**Table 5-1: Planimetric Accuracy Results of SN30 image from 22.02.2023 over Ankara (Absolute, in meter unit).**

Reference	GCP Set
Working Image (SN30 L1 image 1 m)	L1 product of 22.02.2023
Sample (#GCP)	25
Easting Error Mean (m)	0.31
Northing Error Mean (m)	0.08
Easting Error STD (m)	0.90
Northing Error STD (m)	0.84
<b>Easting Root Mean Square Error (m)</b>	<b>0.96</b>
<b>Northing Root Mean Square Error (m)</b>	<b>0.85</b>
<b>Root Mean Square Error (m)</b>	<b>0.90</b>
<b>Circular Error @ 90 Percentile (m)</b>	<b>1.37</b>



**Figure 5-2: GCP Error vectors fields (Ankara test site).**

In addition, 3 UAV orthoimages with very high GSD (3- 5 cm) and corresponding georeferencing accuracy were used as reference. Green bands of the UAV images were matched with the Green band of SN30 data by using the KARIOS tool.

The results indicate large geolocation accuracy variation **within an image** (range between 1.34 m – 2.64 m CE90) see Table 5-2. The effect of topography and land cover is observed in the distribution of local systematic errors. Topographic effects may be removed by using higher resolution DEMs. Currently ESRI image basemap and MapZen DEM products are used as reference for the georeferencing process [RD-5]. The resolutions and accuracy of the products depend on the geographical region.

**Table 5-2. Absolute accuracy results obtained from the matching of SN30 Green band data acquired on 22.02.2023 with respect to reference UAV orthoimages over three image sub-regions.**

Site	RMSE X (m)	$\sigma$ X (m)	RMSE Y (m)	$\sigma$ Y (m)	RMSE XY (m)	CE90 (m)
UAV-1	0.86	0.67	0.66	0.32	<b>1.09</b>	<b>1.61</b>
UAV-2	0.70	0.62	0.49	0.38	<b>0.86</b>	<b>1.34</b>
UAV-3	1.68	0.66	0.69	0.54	<b>1.81</b>	<b>2.64</b>

Figure 5-3 illustrates the discrepancies detected with KARIOS between UAV site 2 and SN30 Green band. The effect of topography and land cover can be observed in the distribution of the errors.

Errors overview

Monitored : Ankara\_SN30\_green\_clip\_uav2.tif  
Reference : UAV\_site2\_1m\_green.tif

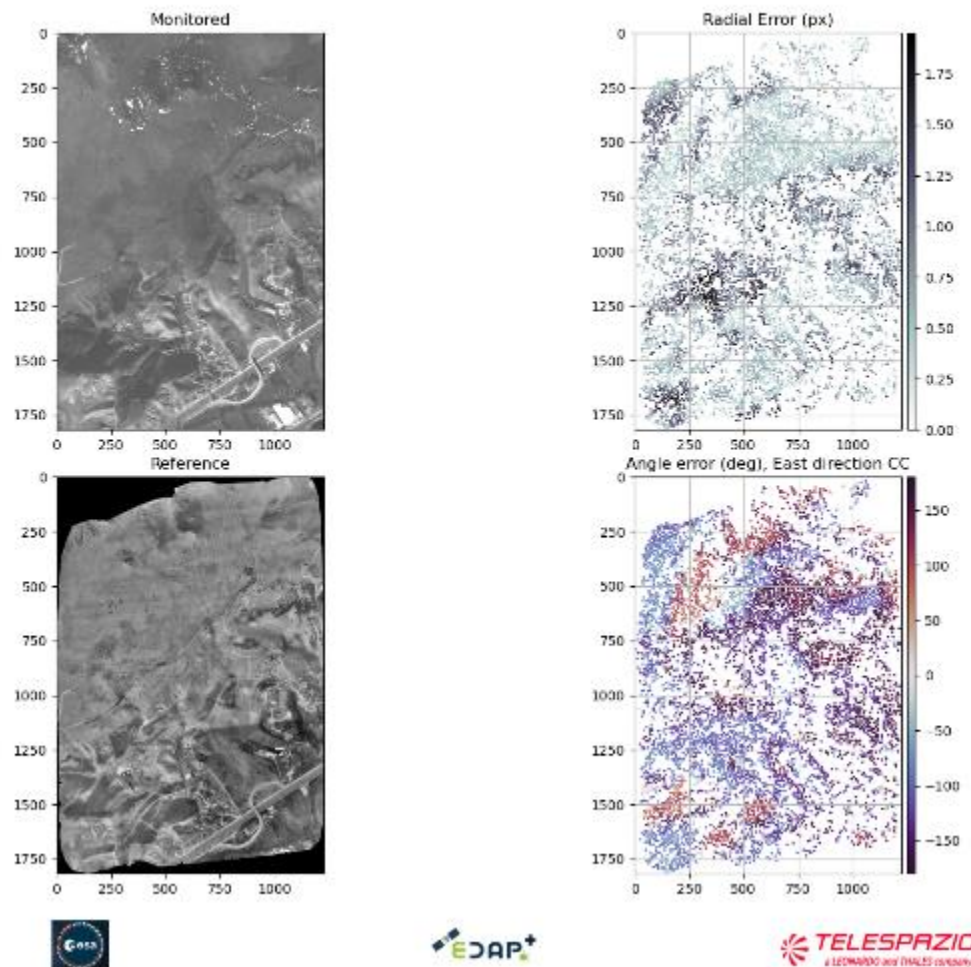


Figure 5-3: KARIOS matching results between SN30 Green band (upper left) and UAV site 2 orthophoto Green band (lower left) images expressed in radial distance as pixels (upper right) and the angular error as degrees (lower right).

## 5.3 Temporal Geolocation Accuracy

### 5.3.1 Methods

The multi-temporal accuracy was evaluated over three different sites: Atacama, Baotou & Gobabeb. L1 products acquired at different dates were matched with the KARIOS tool with sub-pixel accuracy (ca. 0.1 pixel). The results were evaluated with statistical methods and visual assessment.

The assessment was performed on the Green band images and results reported accordingly. The Green band was selected as reference due to its position on the focal plane (closer to the centre). It is worth noting that regarding the other Blue, Green, Red, NIR images, the results on inter-band registration given later in the document can then be used to derive the temporal accuracy for the other spectral bands.

### 5.3.2 Data

**Table 5-3. SN data used for the temporal geolocation assessment**

Site	Acquisition Date	Satellite	Bands
Atacama, Chile	16.12.2022	SN27	Green
	31.12.2022		
Baotou, China	14.06.2022	SN27	Green
	17.06.2022	SN29	
	18.06.2022	SN30	
Gobabeb, Namibia	07.07.2022	SN24	Green
	18.08.2022	SN30	
	18.08.2022	SN29	
	27.10.2022	SN29	
	12.11.2022	SN30	
	16.11.2022	SN30	

### 5.3.3 Results

The results obtained over the three sites are listed in Table 5-4, Table 5-5 and Table 5-6 and all report CE90 values range between 3.2 m to 6.5 m.

The smallest errors were observed between the matching of the same satellite images (e.g. SN27-SN27 or SN30-SN30). All values remain within the absolute accuracy specification (CE90 < 10 m). The distribution of the coordinate discrepancies reveals the effect of the topography and land use in georeferencing.

Along- and across-track systematic errors were observed from the matching of the same satellite data (Figure 5-4). The along-track direction corresponds to Northing and across-track direction corresponds to Easting approximately.

In addition, tiling effect is observed between the data of different satellites (see Baotou and Gobabeb results in Figure 5-5 and Figure 5-6) even taken on the same day (Figure 5-7). The images are processed in a grid structure as tiles as explained briefly in APPENDIX D.

The Figure 5-8 shows the accuracy trends over Gobabeb site, Namibia.

#### Atacama test site

**Table 5-4. Atacama temporal Geolocation Accuracy Results (in meter unit).**

Reference Image (SN27 Green)	16 Dec 2022
Working Image (SN27 Green)	31 Dec 2022
Sample (#Pixel)	59,846
Correlation Confidence	0.90
Easting Error Mean (m)	-2.23
Northing Error Mean (m)	-0.24
Easting Error STD (m)	1.05
Northing Error STD (m)	0.65
<b>Easting Root Mean Square Error (m)</b>	<b>2.46</b>
<b>Northing Root Mean Square Error (m)</b>	<b>0.69</b>
<b>Root Mean Square Error (m)</b>	<b>2.56</b>

Circular Error @ 90 Percentile (m)	3.70
------------------------------------	------

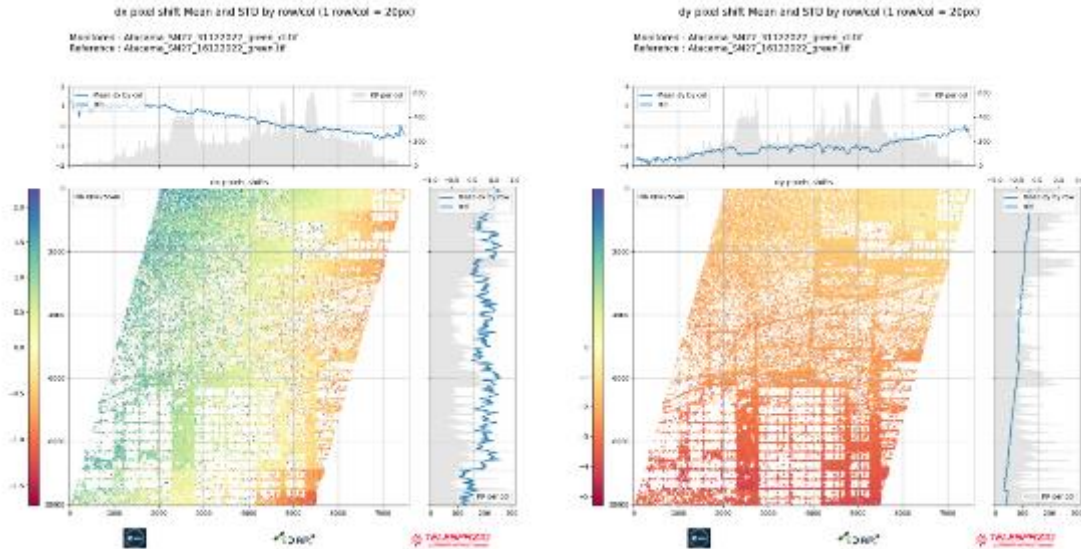


**Figure 5-4: Multi-temporal accuracy assessment results over Atacama site. The discrepancy distribution easting (left) and northing (right) indicate systematic errors in along- and across-track directions.**

Baotou test site

**Table 5-5: Baotou temporal Geolocation Accuracy Results (in meter unit).**

Reference Image (SN27 Green)	14 June 2022
Working Image (SN30 Green)	18 June 2022
Sample (#Pixel)	109,985
Correlation Confidence	0.90
Easting Error Mean (m)	1.64
Northing Error Mean (m)	-2.36
Easting Error STD (m)	1.81
Northing Error STD (m)	1.39
<b>Easting Root Mean Square Error (m)</b>	2.44
<b>Northing Root Mean Square Error (m)</b>	2.74
<b>Root Mean Square Error (m)</b>	3.67
Circular Error @ 90 Percentile (m)	4.95

The discrepancy distribution easting (lower left) and northing (lower right) indicates systematic errors in along- (Northing) and across-track (Easting) directions in Figure 5-5. In addition, effect of image tiles are observed in the northing errors (upper left and lower right figures).

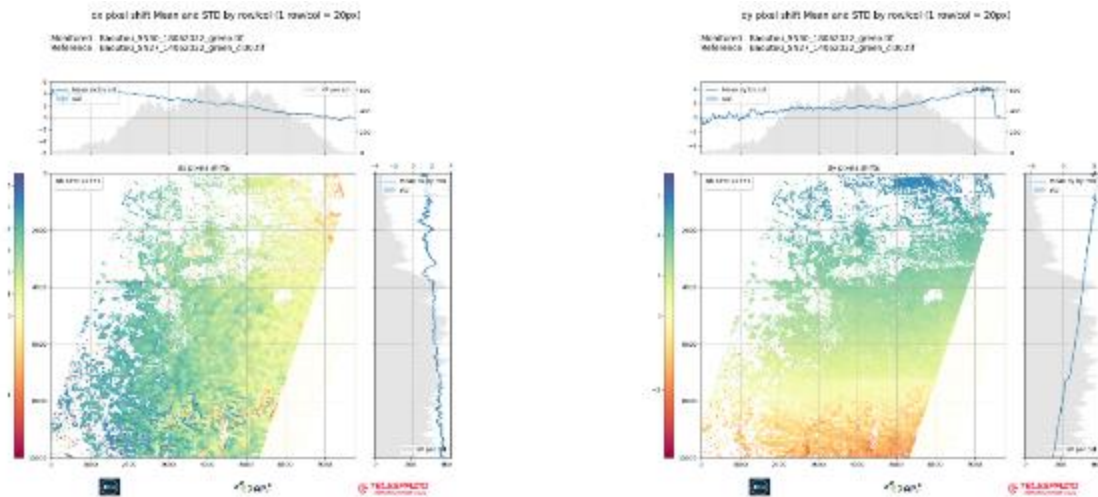
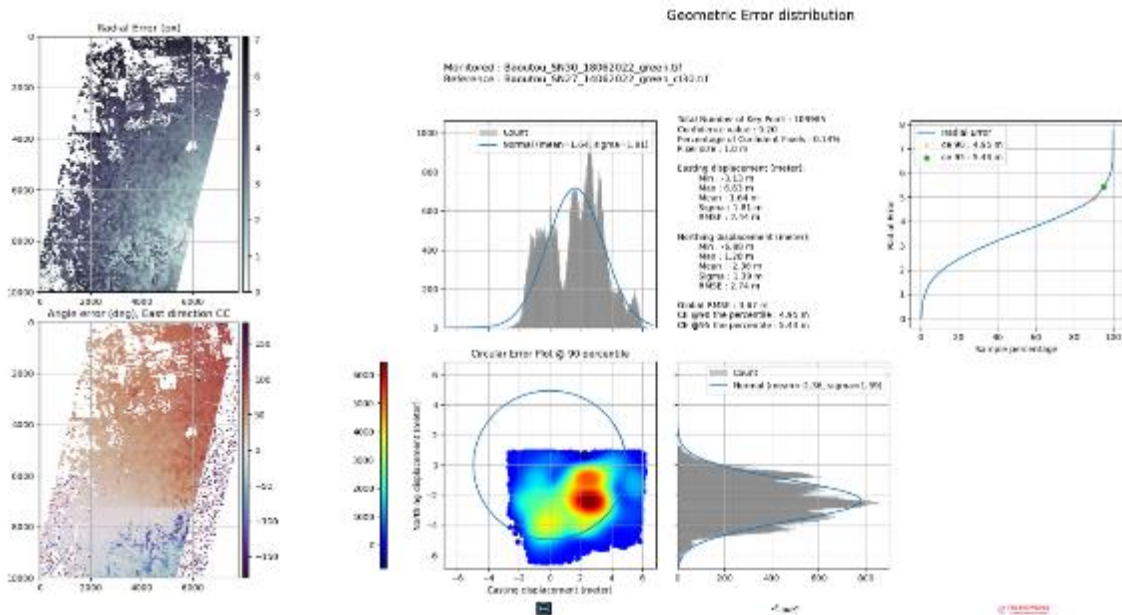


Figure 5-5: Multi-temporal accuracy assessment results over Baotou site.

Table 5-6. Gobabeb multi-temporal image analysis results. SN30 (18 August 2022) Green band image was taken as reference.

Satellite data	RMSE X (m)	$\sigma$ X (m)	RMSE Y (m)	$\sigma$ Y (m)	RMSE XY (m)	CE90 (m)
SN30 16.11.2022	1.0	1.0	1.7	1.6	2.0	3.2
SN30 12.11.2022	1.6	1.0	2.2	1.5	2.7	3.7
SN29 27.01.2022	4.4	2.4	2.8	2.0	5.2	6.5

SN24 07.07.2022	4.0	2.7	2.4	2.2	4.6	6.3
SN29 18.08.2022*	3.6	1.5	1.6	1.6	3.9	4.8

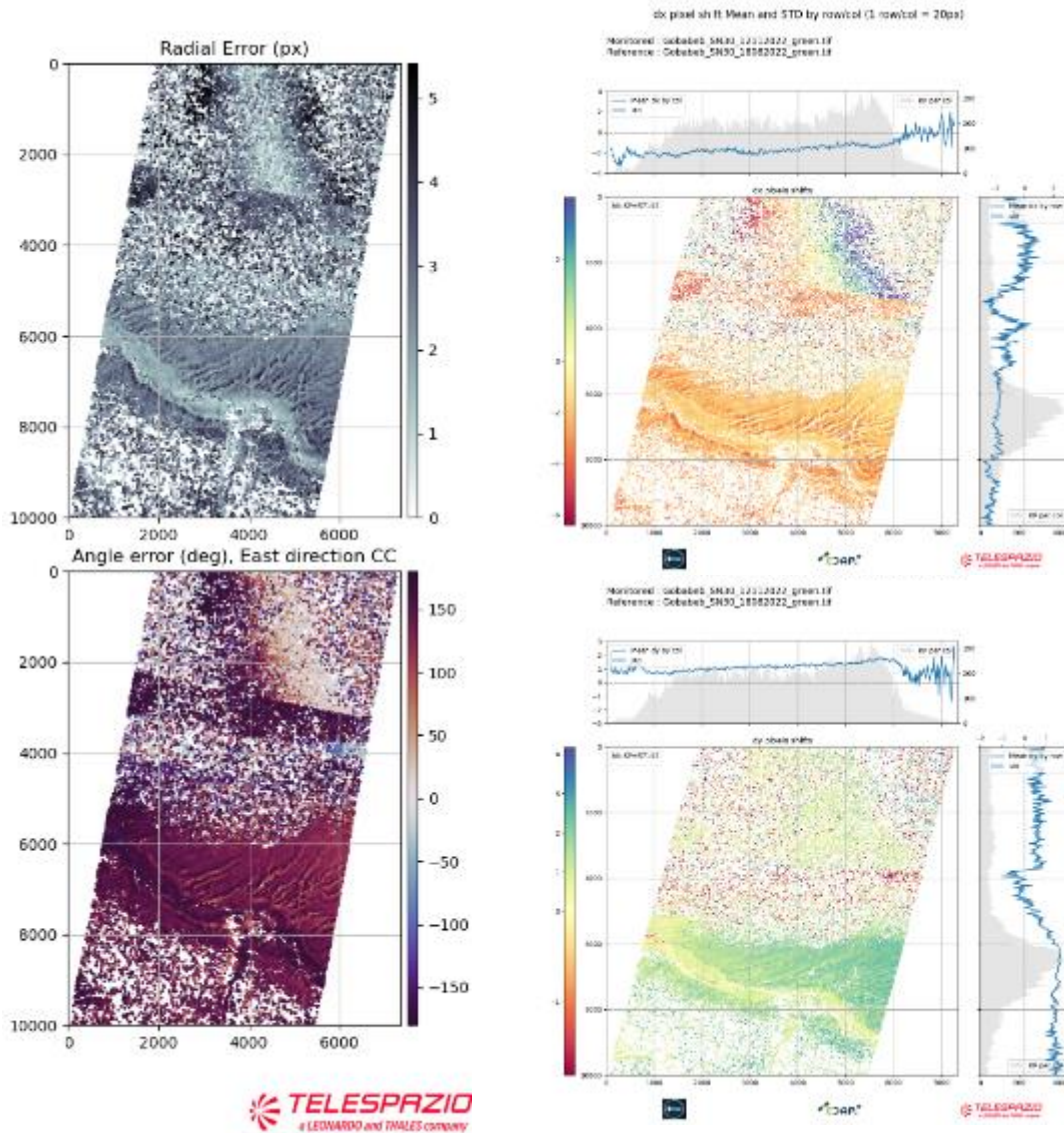


Figure 5-6: Image coordinate differences obtained from matching over Gobabeb site between SN30 images taken on 18 August 2022 (reference image) and 12 November 2022 (working image). Effect of topography and land cover is visible on the results.

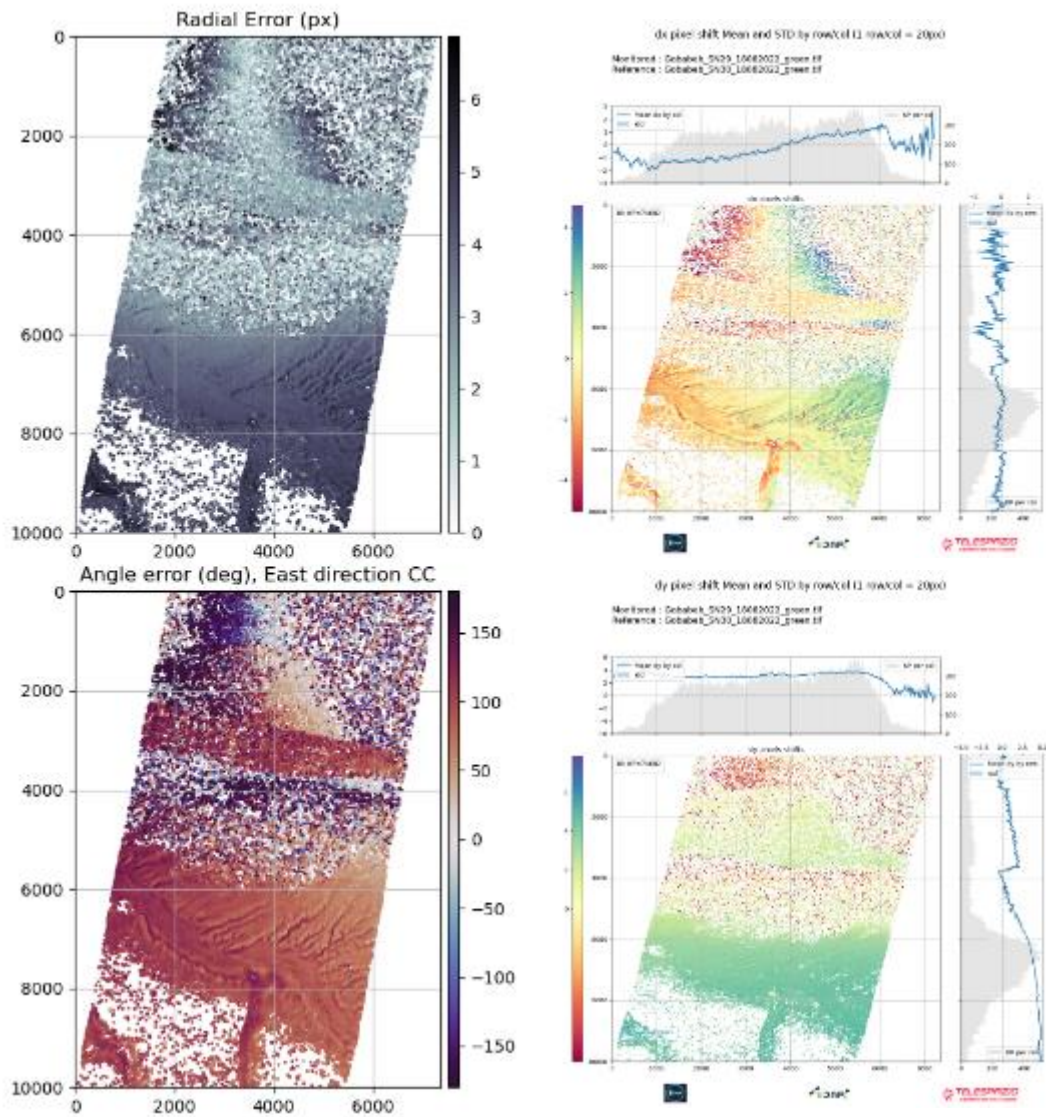


Figure 5-7: Image coordinate differences obtained from matching of the same day images from SN29 and SN30 taken on 18 August 2022 over Gobabeb site

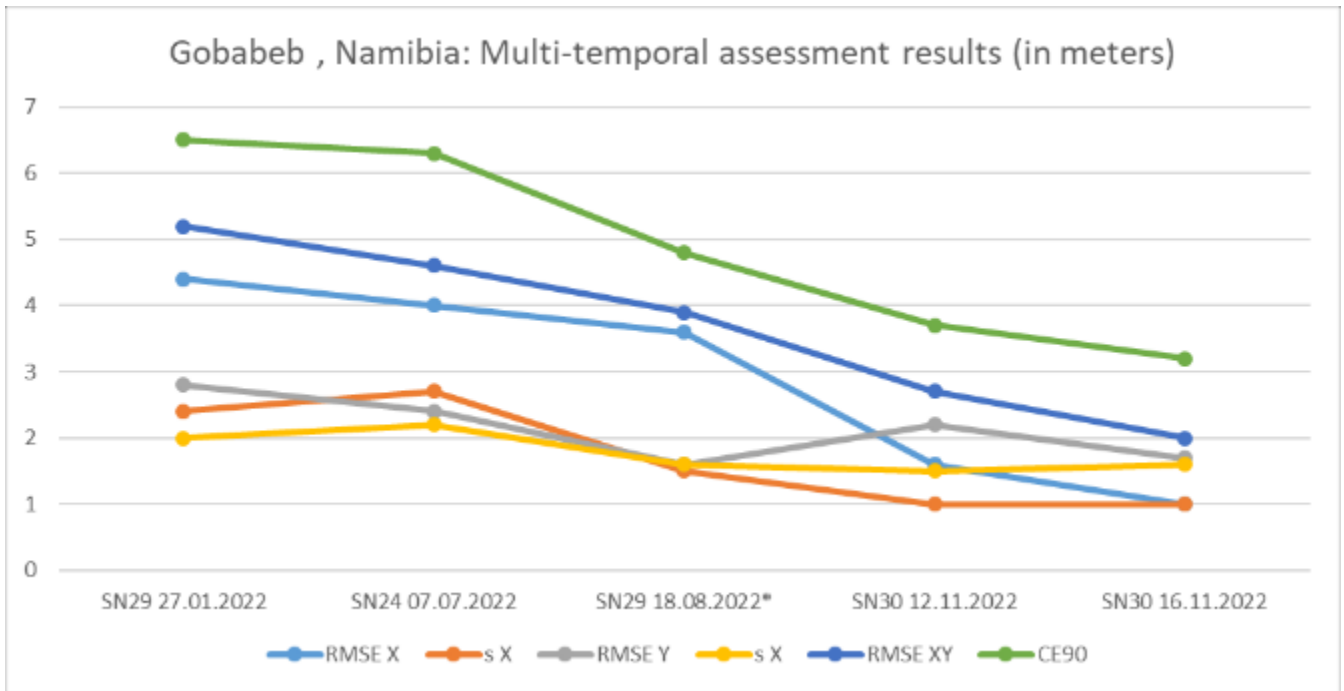


Figure 5-8: Multi-temporal accuracy assessment results over Gobabeb, Namibia. N30 (18 August 2022) Green band image was taken as reference

## 5.4 Inter-band Registration Accuracy

### 5.4.1 Methods

The objective is to assess the co-registration between bands. For a given product, several band twins are considered, namely (Green, Blue), (Green, Red), (Green, NIR), and the geometry of the two image grids in the twin, are compared. The grids are compared by using a dense image matching technique: for any pixel location in the image space, a displacement,  $D$ , in both line ( $y$ ) / pixel ( $x$ ) direction, is computed.

The post processing of image matching results is an essential stage before producing accuracy statistics and the related error budget.

### 5.4.2 Data

Ankara, Atacama, and Baotou L1 datasets (orthorectified) were assessed for inter-band accuracy.

Table 5-7. Data used to assess the inter-band accuracy.

Site	Dates	Satellites
Ankara, Turkey	30.12.2022 22.02.2023	SN27 SN30
Atacama, Chile	16.12.2022 31.12.2022	SN27
Baotou, China	14.06.2022 17.06.2022 18.06.2022	SN27 SN29 SN30

### 5.4.3 Results

The results listed in Table 5-8 indicate an uncertainty that varies depending on the selected validation test site.

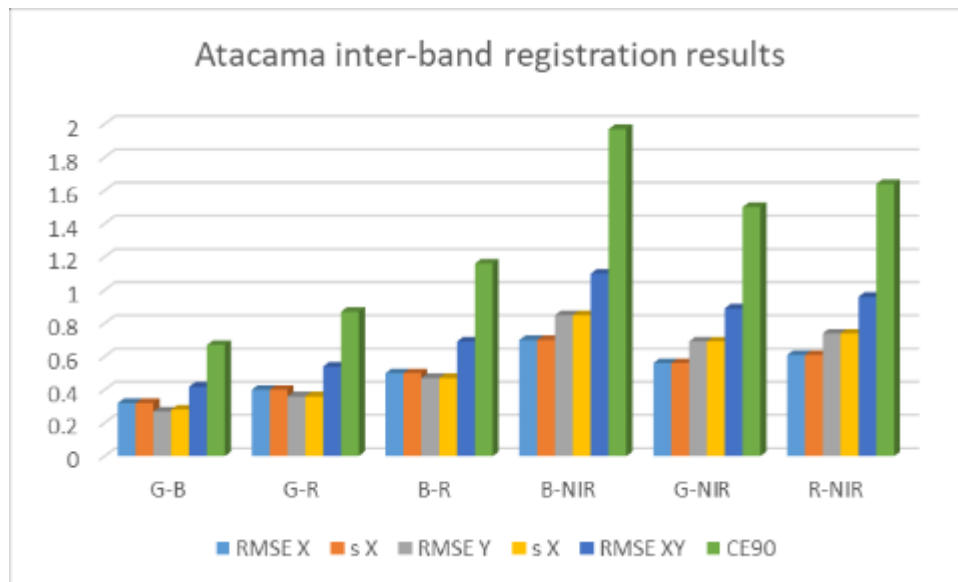
The matching between the Green and NIR bands revealed large inter-band errors for the NIR band (up to 1.1 pixel  $RMSE_{XY}$ ).

**Table 5-8: Inter-band registration results.**

Site & Data	Band twin	RMSE X (m)	$\sigma$ X (m)	RMSE Y (m)	$\sigma$ Y (m)	RMSE XY (m)	CE90 (m)
Ankara SN30 L1	G-B	0.16	0.16	0.15	0.15	0.22	0.34
	G-R	0.14	0.14	0.13	0.13	0.19	0.29
	G-NIR	0.21	0.21	0.19	0.19	0.44	0.51
Ankara SN27 L1	G-B	0.17	0.17	0.14	0.14	0.22	0.34
	G-R	0.16	0.16	0.12	0.12	0.20	0.30
	G-NIR	0.31	0.25	0.19	0.19	0.36	0.55
Baotou SN27 14 June L1	G-B	0.22	0.22	0.22	0.22	0.31	0.48
	G-R	0.18	0.18	0.17	0.17	0.25	0.38
	G-NIR	0.41	0.26	0.36	0.26	0.55	0.80
Baotou SN29 17 June L1	G-B	0.37	0.37	0.37	0.36	0.53	0.82
	G-R	0.24	0.24	0.23	0.23	0.33	0.52
	G-NIR	0.46	0.46	0.40	0.40	0.61	0.98
Baotou SN30 18 June L1	G-B	0.22	0.22	0.25	0.25	0.33	0.51
	G-R	0.16	0.15	0.16	0.15	0.22	0.34
	G-NIR	0.25	0.24	0.24	0.23	0.35	0.53
Atacama SN27 16 Dec L1	G-B	0.22	0.22	0.21	0.21	0.31	0.49
	G-R	0.23	0.23	0.22	0.22	0.32	0.51
	G-NIR	0.27	0.30	0.27	0.28	0.40	0.64
Atacama SN27 31 Dec L1	G-B	0.32	0.32	0.27	0.28	0.42	0.67
	G-R	0.40	0.40	0.36	0.36	0.54	0.87
	B-R	0.50	0.50	0.47	0.47	0.69	1.16
	B-NIR	0.70	0.70	0.85	0.85	1.10	1.97
	G-NIR	0.56	0.56	0.69	0.69	0.89	1.50

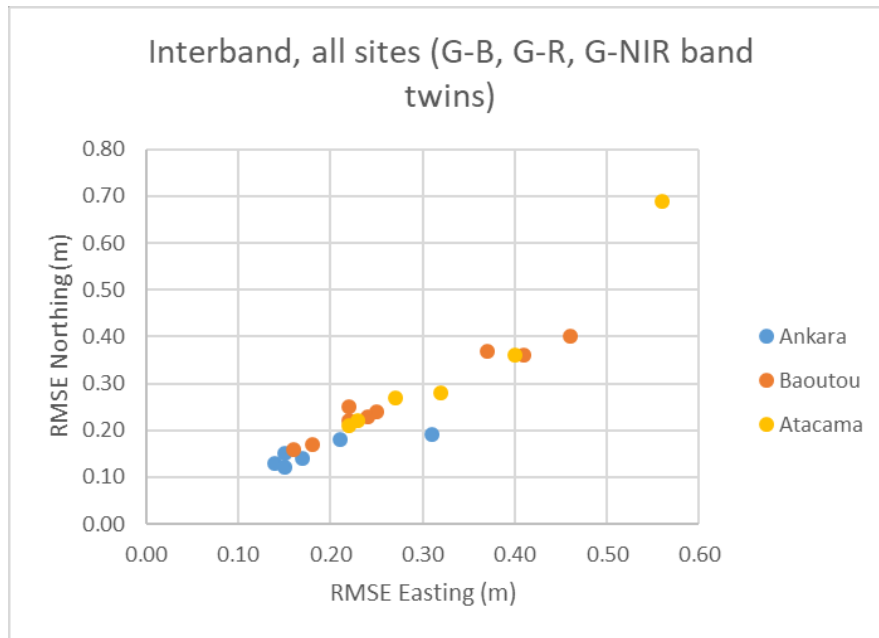
Site & Data	Band twin	RMSE X (m)	$\sigma$ X (m)	RMSE Y (m)	$\sigma$ Y (m)	RMSE XY (m)	CE90 (m)
	R-NIR	0.61	0.61	0.74	0.74	0.96	1.64

Figure 5-9 shows the statistical results over the Atacama site for different bands. The RMSE XY values exceed the specification (0.3 pixel) in some cases. The results are however compliant with the data provider results ( $0.7 \pm 0.39\sigma$  pixel). It is worth noting that the data provider considers the larger errors as a limitation to the algorithm used.



**Figure 5-9: Inter-band accuracy assessment results (m), Atacama 31 December 2022 SN27.**

A graphical representation of interband results from all sites in terms of RMSE northing and Easting is shown in Figure 5-10. From the figure, it can be observed that there are variations in interband accuracy between sites and datasets.



**Figure 5-10: Interband results for all sites**

Figure 5-11 shows coordinate discrepancy plots expressed as angular and radial errors between blue and NIR band images of SN27 taken on 31.12.2022. The northern part of the images show even greater discrepancy that can be associated with the image chip processing and the land cover type. Image tile processing effect is also observed in the figure.

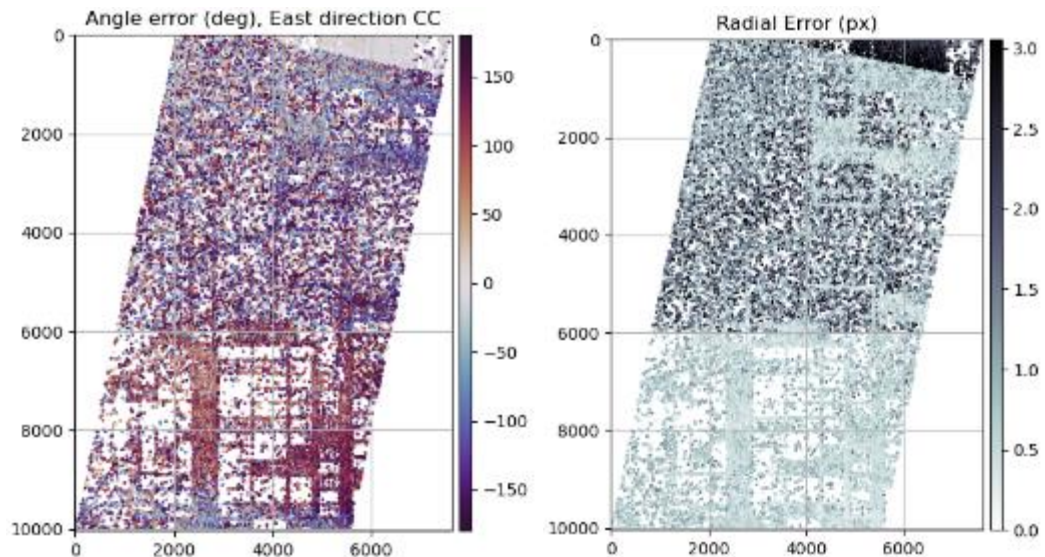


**Figure 5-11: Interband discrepancy plots (angular and radial errors) over Atacama site obtain from the matching between blue and NIR bands of SN27 image taken on 31.12.2022.**

## 5.5 Results Compliance

Three critical validation items have been checked for geometric calibration and validation: the absolute accuracy, the temporal accuracy, and the inter-band registration accuracy. The geometric calibration of SN27 and SN30 has been validated for absolute, temporal and inter-band accuracy. In addition, SN24 and SN29 were evaluated for temporal accuracy. Further inter-band tests were carried out for SN29 as well.

**Table 5-9: Satellogic NS / EDAP – comparison of Uncertainty Results.**

	Inter-band Mean Accuracy [m], (#7 Products)	Absolute Geolocation Mean Accuracy [m], (#1 product)	Temporal Geolocation Mean Accuracy [m], (#7 products)
EDAP +	Green-Blue: 0.33 RMSE / <b>0.52</b> CE90  Green - Red: 0.29 RMSE / <b>0.49</b> CE90  Green -NIR: 0.49 RMSE / <b>0.78</b> CE90	1.17 RMSE <b>1.74</b> CE90	3.53 RMSE 4.73 CE90
Satellogic [RD-5]	Current performance: <b>&lt;0.70</b> CE90 (Target: 0.3)	Current performance <b>&lt;11.8</b> CE90 (Target: 10 m )	<i>Not available</i>

### 5.5.1 Absolute Geolocation Accuracy

The absolute geolocation accuracy was computed using one SN30 product over the Ankara site. 25 GCPs covering the full extent of the product taken on 22.02.2023 and 3 UAV acquisitions covering sub-parts of the same product were used for the evaluations. The ground-surveyed GCPs were manually measured in the L1 RGB image. L1 and L3 products have the same geometry definitions. The three UAV orthophotos were used as reference in the image matching tool working with least-squares area matching principle.

For the absolute accuracy validation items, the results were found in agreement with the accuracy specifications (<10 m CE90) given by the data provider in [RD-3] and the results (6.5 m CE95) given in the USGS System Characterization Report on the Satellogic NS Multispectral Sensor [RD-11]. The maximum CE90 value was found 2.64 m based on Ankara site evaluations with UAV data. The evaluations with GCPs yielded 1.37 m CE90 values over Ankara test site. These results are compliant with the product specifications.

Thus, the absolute geolocation accuracy grade for L1 and L3 products is “excellent”.

### 5.5.2 Temporal Geolocation Accuracy

The temporal accuracy results were evaluated over Gobabeb, Baotou and Atacama sites using 10 products from SN24, SN27, SN29 and SN30 satellites. Same day images from different satellites and same satellite images were also compared.

The results show that the global differences are within the absolute accuracy specifications given by the data provider (< 10 m CE90). The maximum difference was 6.5 m CE90 over Gobabeb. Discrepancy plots obtained from the dense image matching results revealed the effects of image tiling, land cover and topography in their distributions.

The temporal geolocation accuracy grade for L1 and L3 products is “excellent” due to the large discrepancies between the images over rugged topography.

### 5.5.3 Inter-band Geolocation Accuracy

The inter-band accuracy was calculated using seven L1 products taken over three sites (Ankara, Baotou, Atacama) with SN27, SN29 and SN30. The green band was taken as reference to be compared with Blue, Red and NIR bands. Further investigations between Red-NIR, Blue-NIR and Red-Blue were carried out over the Atacama site due to large errors.

The results show that the inter-band accuracy is not stable over different bands and sites, being the NIR band with the poorest accuracy results. Temporal differences between the bands affect the accuracy causing the largest differences between the Blue and NIR bands as they have the largest time interval between the acquisitions. Effects of image tiling, land cover and topography were also observed in the inter-band evaluations. Potential band-to-band registration issues due to sensor optical design and moving objects (clouds, vehicles, etc.) were already expected. Relative geometric calibration and image inner accuracy investigations may be needed due to potential camera optical distortions.

The inter-band results show misregistration errors up to 2 m CE90 between Blue and NIR bands. Closely located bands revealed errors at smaller magnitudes.

The inter-band geolocation accuracy grade for L1 and L3 products is “good”.

## 6. DETAILED VALIDATION – RADIOMETRY

### 6.1 Introduction

The radiometry of NS images has been assessed based on two methods, a vicarious calibration method considering reference fiducial data from RCN network and a cross calibration method considering PICS sites and Sentinel-2 data.

### 6.2 Absolute Calibration Accuracy

#### 6.2.1 Method

The method used to determine the absolute radiometric calibration accuracy of the sensor's channel is based on comparing the top-of-atmosphere reflectance values derived from the sensors acquisitions of the chosen RadCalNet calibration sites with the simulated top-of-atmosphere reflectance values.

The RadCalNet calibration sites, operated by the Committee on Earth Observation Satellite (CEOS) Working Group for Calibration and Validation (WGCV) InfraRed and Visible Optical Sensors (IVOS), provides the scientific community with the following:

- Simulated Top-of-atmosphere reflectance values (MODTRAN), derived from both in-situ surface and atmosphere measurements (e.g., surface pressure, columnar water vapour, columnar ozone, aerosol optical depth, etc.) that are SI-traceable, at:
- 30-minute intervals between 09:00 and 15:00 local standard time (cloud-free data only), and 10 nm spectral sample intervals between 400 nm and 1000 nm.

As mentioned in <sup>6</sup>, the RadCalNet simulated top-of-atmosphere reflectance spectra are representative nadir view observations only. Comparison to space sensor reflectance measurements should be exercised with caution when the sensor viewing zenith angle deviates significantly from nadir as both atmospheric and surface non-Lambertian behaviour can lead to significant deviation from at nadir simulated signal.

For some TDS products, the sensor viewing zenith angle can be up to 14° (Table 6-2). Therefore, comparison with RCN has been performed through Bidirectional Reflectance Distribution Function (BRDF) normalization step. One year of Sentinel-2 TOA data has been collected and BRDF VJB parameters invert, using the High Resolution Adjusted BRDF Algorithm (HABA) ([RD-16]). BRDF normalization step considers Li Sparse kernel for Geometric component and the Modified Roujean kernel for Volumetric component.

Finally, the percentage difference between sensor top-of-atmosphere reflectances ( $\rho_b work$ ) and simulated sensor top-of-atmosphere reflectances ( $\rho_b simulated$ ), using RadCalNet data, is calculated as follows:

$$\rho_b = ((\rho_b simulated - \rho_b work) / (\rho_b simulated)) * 100$$

A simple ratio,  $\rho_b simulated / \rho_b work$  is also report.

---

<sup>6</sup> [https://www.radcalnet.org/resources/RadCalNetQuickstartGuide\\_20180702.pdf](https://www.radcalnet.org/resources/RadCalNetQuickstartGuide_20180702.pdf)

## 6.2.2 Data

The following table details the input dataset involved in the vicarious calibration exercise. The input dataset delivered by the data provider includes many products observed over RCN sites. Unfortunately for a few of them, RCN simulated data (TOA) is available at NS overpass time.

**Table 6-1: Test dataset for vicarious calibration exercise.**

Product	RCN site	Satellite	Obs Date	Obs Time (UTC)	DOY
20220707_094842_SN24_L1	GONA	SN24	07/07/2022	09:48:42.9	188
20221027_115607_SN29_L1	GONA	SN29	27/10/2022	11:56:07.4	300
20221116_115217_SN30_L1	GONA	SN30	16/11/2022	11:52:18.0	320
20220707_211429_SN29_L1	RVUS	SN29	07/07/2022	21:14:29.2	188
20220630_211430_SN29_L1	RVUS	SN29	30/06/2022	21:14:30.8	181

The following table details the geometries of observation, essential parameters used to appreciate the results and model directional effects. One can observe variation in NS Viewing Zenith Angle (**VZA**) and Viewing Azimuth Angle (**VAA**) the VZA of NS observation can be up to 15 degrees. Taking into account that RNC TOA simulation are given at Nadir (0 degree), the direct comparison includes within this condition many uncertainties.

**Table 6-2: Geometries of Vicarious calibration dataset.**

Product	Solar Zenith Angle(°)	Solar Azimuth Angle(°)	Viewing Zenith Angle(°)	Viewing Azimuth Angle(°)	Water Vapour (g/cm)	AOD
20220707_094842_SN24_L1	49.69	23.11	<b>14.36</b>	278.59	1.030	0.076
20221027_115607_SN29_L1	20.32	298.71	2.72	93.22	3.027	0.0957
20221116_115217_SN30_L1	16.57	283.65	<b>10.31</b>	97.11	1.016	0.0425
20220707_211429_SN29_L1	24.49	235.51	4.88	100.93	0.933	0.0479
20220630_211430_SN29_L1	24.23	237.05	5.40	101.49	1.106	0.0897



**Figure 6-1: GONA NS L3 Images.**

### 6.2.3 Results

This radiometric calibration validation activity shows that accuracy of NS family is conformed to the claimed specification: all validation results are within accuracy ranges given by the data provider (< 10%), as shown in Table 6-3, Table 6-4, Table 6-5 and Table 6-6. Table 6-5 and Table 6-6 indicate results including BRDF normalization step.

**Table 6-3: NS / RCN Inter calibration Ratio.**

	NS TOA /RCN TOA			
	Blue	Green	Red	NIR
20220707_094842_SN24_L1	0.97	0.97	0.94	0.98
20221027_115607_SN29_L1	0.97	0.97	0.98	1.01
20221116_115217_SN30_L1	0.96	0.99	0.95	0.97
20220707_211429_SN29_L1	0.95	0.96	0.93	1.00
20220630_211430_SN29_L1	0.94	0.94	0.95	0.98

**Table 6-4: NS / RCN Inter calibration Percent difference.**

	NS TOA/RCN TOA (Percent difference)			
	Blue	Green	Red	NIR
20220707_094842_SN24_L1	3.39%	2.57%	5.57%	1.89%
20221027_115607_SN29_L1	2.68%	3.06%	2.10%	-1.12%
20221116_115217_SN30_L1	4.03%	1.15%	5.38%	3.00%
20220707_211429_SN29_L1	5.07%	4.19%	6.93%	-0.04%
20220630_211430_SN29_L1	5.82%	5.78%	4.78%	1.90%

**Table 6-5: NS / RCN Inter calibration Ratio with BRDF normalisation.**

	NS TOA/RCN TOA (BRDF Normalisation)			
	Blue	Green	Red	NIR
20220707_094842_SN24_L1	0.98	0.99	0.95	0.99
20221027_115607_SN29_L1	0.98	0.98	0.99	1.02
20221116_115217_SN30_L1	1.00	1.03	0.98	1.00

**Table 6-6: NS / RCN Inter calibration percent difference with BRDF normalisation.**

	NS TOA/RCN TOA Percent difference (BRDF Normalization)

	Blue	Green	Red	NIR
20220707_094842_SN24_L1	1.96%	1.05%	4.53%	0.79%
20221027_115607_SN29_L1	1.75%	2.09%	1.32%	-1.94%
20221116_115217_SN30_L1	0.18%	-2.82%	2.28%	-0.26%

## 6.3 Temporal Stability

### 6.3.1 Method

The scope of the temporal stability method is to validate vicarious calibration results. A straightforward method based on PICS sites is used. A temporal stability of radiometric calibration is expected, considered as reference one product in the delivered TDS. There is no specification from the data provider but a variation with 10% is expected. The temporal variation is also analysed by using comparison with S2 data.

The PICS sites are referenced by the CEOS (for their utility in radiometric calibration / validation activities). Among PICS, the Libya-4 test site is used. The site is located in the Libyan Desert in Africa at coordinates +28.55° N and +23.39° W, with a terrain elevation of about 118 m above sea level.

The Libya-4 site was first proposed for the SPOT calibration [RD-17] and demonstrated potential to be utilised for low, medium and high resolution optical visible and near infrared data [RD-19], [RD-20], [RD-21], [RD-22]. This site is categorised as a “bright” site. As discussed in [RD-23], within the context of reflectance-based methods, this site is characterised by high reflectance in conjunction with low aerosol loading and a predominance of clear skies that reduces the impact of atmospheric errors. Other important aspects are the near Lambertian reflectance, the spectral and spatial uniformity and the temporal stability.

The temporal stability of NS ROI method has been assessed by using two years of S2 data (34RGS). Variations of TOA measurements with respect to scattering angles have been analysed and used to invert a model as shown in Figure 6-2. Residual errors of adjustment are essentially due to meteorological conditions. R square results demonstrate that as a first approximation, the use of a linear model is justified, R square is above 0.6 in most cases. Based on NS observation, geometries are then used as input of the model to predict S2 reference TOA values.

Finally, the percentage difference between NS TOA reflectances ( $\rho_b work$ ) and S2 simulated sensor top-of-atmosphere reflectances ( $\rho_b simulated$ ), using site characterization data, is calculated as follows:

$$\rho_b = ((\rho_b s2\_simulated - \rho_b NS) / (\rho_b s2\_simulated)) * 100$$

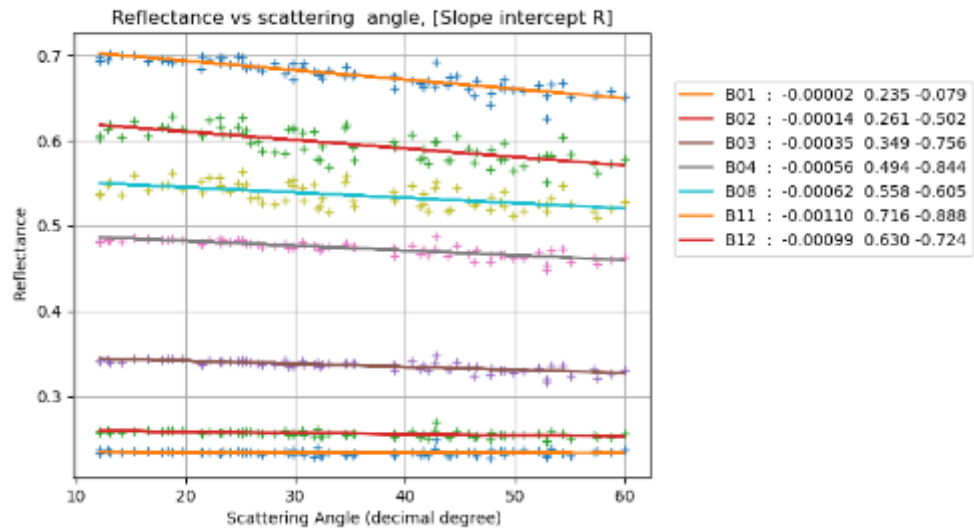


Figure 6-2: TOA Angular dependency of NS ROI (S2 / MSI)

### 6.3.2 Data

As shown in the Figure 6-3, a small ROI corresponding to NS tile '1 – 4'. The extent of this ROI is 4 km x 4 km. This ROI is small compared to one used in CEOS PICSCAR exercise.

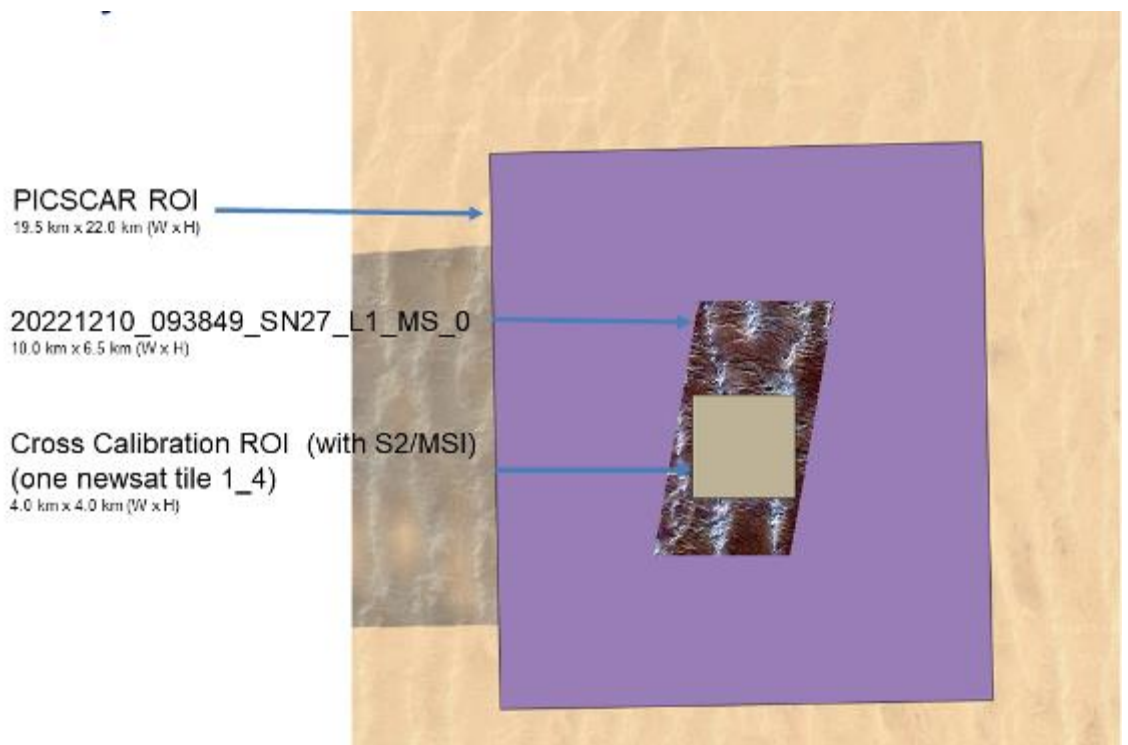


Figure 6-3: Libya 4 site and NS ROI definition

This assessment is based on three Level 1 products observed in Winter 2022/2023, with two different spacecraft (SN#27 / SN#29), at the following dates / time:

- 10/12/2022 09:38:49 - 20221210\_093849\_SN27\_L1,

- 09/01/2023 09:37:41 - 20230109\_093740\_SN27\_L1,
- 09/01/2023 11:52:59 - 20230109\_115258\_SN30\_L1.

Please refer to APPENDIX B for details regarding the TDS.

At this scale, the region of interest displays one large longitudinal dune, with varying illumination nearby the dune, depending on observation conditions (time, relative position), as shown in Figure 6-3. It is a reason for which, performing cross comparison between measurements is not straightforward.

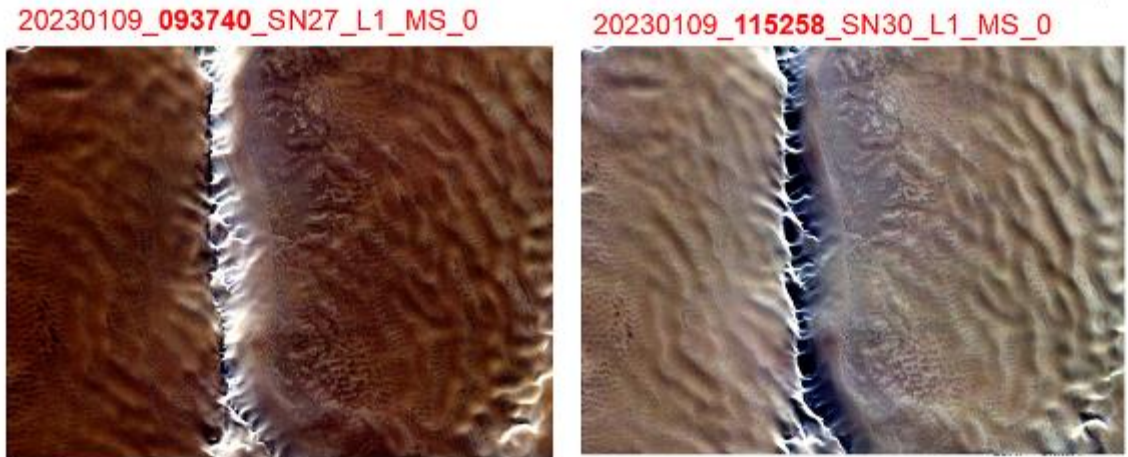


**Figure 6-4: Detailed on Libya 4 NS ROI through NS#27 / NS#30 RGB image comparison**

A time series of Sentinel-2 data (34RGS Data, year 2022 / year 2023) yielded to the characterization of the ROI in term of calibration stability. As anticipated, TOA measurements are extremely stable in time, as shown in Figure 6-5. Inter season variations are observed due to water vapour content in particular for Red and NIR channels.

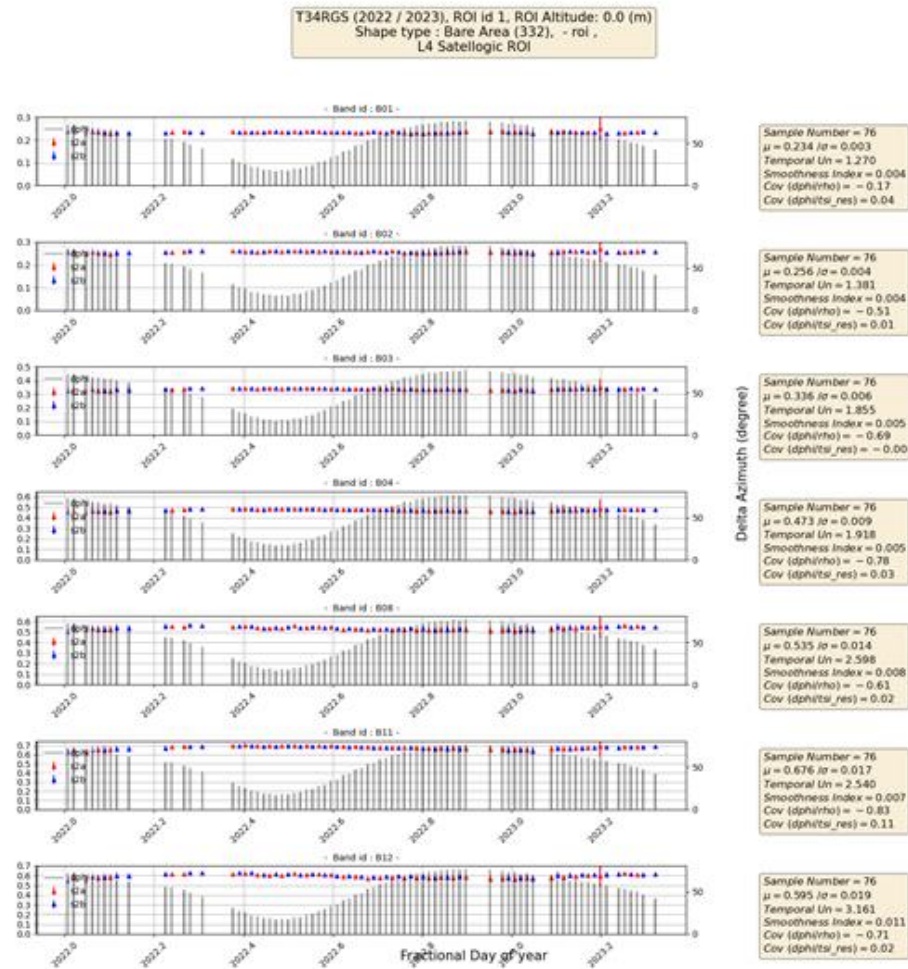


Figure 6-5: Stability of S2 TOA measurements over Libya 4 NS ROI.

As discussed previously, a linear relationship exists between measurements and observation geometries, scattering parameter being exhaustive in this case. For every product, the geometries of observation at the centre of tile ('1\_4') for the three products are listed in Table 6-7.

Table 6-7: NS Geometries of Libya observations

	SZA (dd)	SAA (dd)	VZA (dd)	VAA (dd)	Scattering Angle (dd)
20221210_093849_SN27_L1	52.35	168.28	4.35	266.63	53.10
20230109_093740_SN27_L1	52.38	163.66	1.67	265.29	52.74
20230109_115258_SN30_L1	54.14	202.90	5.12	276.76	52.87

### 6.3.3 Results

The cross-calibration results with S2 data, listed in Table 6-8, are within 8% for all channels. These results reflect spectral differences between NS / S2 sensors. Differences are on the order of Spectral Band Adjustment Factors (SBAF) values found over GONA RCN site. As written in APPENDIX D, for Blue, Green, Red, NIR channels, the SBAF values (% differences) are respectively 0.84%, 4.98%, 7.23% and 3.65%. Accounting for precision of SBAF over GONA results (APPENDIX D), accuracy results found previously with RCN method is confirmed.

**Table 6-8: NS / S2 Cross Calibration (No SBAF Applied).**

	NS TOA/S2 TOA Percent difference (BRDF Normalization)			
	Blue	Green	Red	NIR
20221210_093849_SN27_L1	-0.35%	4.80%	7.35%	3.73%
20230109_093740_SN27_L1	2.58%	6.52%	7.58%	2.18%
20230109_115258_SN30_L1	-1.87%	1.77%	4.47%	-1.42%

As shown in Table 6-9, the temporal stability of measurement is within  $\pm 3.00\%$  for a same mission and  $\pm 5.3\%$  when considering SN27 / SN29. Observation dates are very close, but meteorological conditions and geometries are varying, it is difficult to state on cross calibration accuracy between missions. More data is required.

**Table 6-9: Multi-temporal stability, against 20221210\_093849\_SN27\_L1.**

	Percent difference Against first date (20221210_093849_SN27_L1)			
	Blue	Green	Red	NIR
20230109_093740_SN27_L1	2.90%	1.76%	0.21%	-1.66%
20230109_115258_SN30_L1	-1.53%	-3.21%	-3.14%	-5.38%

## 6.4 Results Compliance

Due to varying geometries, the BRDF normalization step is essential to really appreciate radiometric calibration. Based on a few products observed over RCN site and PICS Libya 4, it is noted that the radiometric calibration accuracy of NS data is compliant with the specification claimed by the data provider [5%-15%]. More elaborate methods over RCN / GONA confirm results. Furthermore, cross calibration with S2 over PICS provides satisfactory results, accounting for spectral differences between both instruments.

As field of investigation, the calibration accuracy of 20220707\_094842\_SN24\_L1 is somehow degraded when comparing with other missions (5% in the Red channel), It raises the point of lifetime model and detector ageing.

The cross calibration between missions might also be investigated by using more data; variations over PICS have been observed to be mitigated with limitations inherited to the



proposed method. Furthermore, requesting TDS including products with a same processing baseline might have been of interest for a more accurate characterization.

## **APPENDIX A NS MISSION**

The ÑuSat (Aleph-1) satellite series is operated by Argentinean company Satellogic for the collection of Earth image products to be made available on the commercial market.

Developed and built by Satellogic S.A, the ÑuSat spacecraft are 43 x 45 x 75 centimeters in size and weigh 37 Kilograms. The microsatellite bus and its imaging payload were tested as part of the BugSat-1 mission launched in 2014.

The satellites carry an imaging system operating in the visible and near InfraRed spectrum, generating still imagery and video of Earth at a ground resolution of up to one meter.

There are two imaging payloads providing high spatial resolution multi spectral and hyperspectral data.

Market: to provide short turnovers from the request of imagery to their delivery, also supporting rapid re-visit times.

Level 1B image is not delivered to the user and its size for one evaluated product (one 2D Array) frame is approximately 1720 x 5385 pixels. L1B image is geolocated but not orthorectified.

L1 / L3 Raster images have the same geometry. Both products are orthorectified. L3 is derived from L1 by applying radiometric stretching, more convenient for image analytics.

## APPENDIX B Mission Test Dataset

Table 6-10: NS Test dataset

Site	SW Version	Satelogic Product Identifier (L1 <sup>7</sup> )	Section
La Crau, France, (43.56 N, 4.86 E)	0_50_8	20220802_131635_SN30_L1	N/A
	0_52_0	20220731_131959_SN29_L1	
	0_52_1	20220805_110735_SN24_L1	
	0_52_0	20221107_131609_SN29_L1	
Railroad Valley Playa, U.S.A., (38.497 N, -115.69 W)	0_52_0	20220513_190614_SN24_L1	6.2
	0_52_1	20220630_211430_SN29_L1	
	0_50_0	20220707_211429_SN29_L1	
Baotou, China, (40.87 N, 109.62 W)	0_50_1	20220618_062155_SN30_L1	4.3, 5.3, 5.4
	0_52_1	20220617_061636_SN29_L1	
Salon-de-Provence, France, (43.61 N, 5.12 E)	0_52_0	20221017_110251_SN27_L1	4.3
	0_52_0	20221104_131432_SN30_L1	
Libya-4, Libya (28.55 N, 23.39 E)	0_50_6	20230109_115258_SN30_L1	4.4, 6.3
	0_50_6	20230109_093740_SN27_L1	
	0_52_4	20221210_093849_SN27_L1	
Ankara, Turkey, (39.9 N, 32.9 E)	0_52_4	20221230_090555_SN27_L1 20230222_112156_SN30_L1	4.2, 5.2, 5.4
Gobabeb, Namibia, (-23.60 S, 15.12 E)	0_52_1	20221116_115217_SN30_L1	5.3, 6.2
	0_50_8	20221112_115357_SN30_L1	
	0_50_8	20220818_115744_SN30_L1	
	0_52_0	20220707_094842_SN24_L1	
	0_50_8	20220818_120136_SN29_L1	
	0_50_8	20221027_115607_SN29_L1	
Atacama, Chile, (-23.51 N, -68.39 E)	0_50_8	20221216_151434_SN27_L1	5.3, 5.4
	0_50_8	20221231_151429_SN27_L1	

<sup>7</sup> L3 products are also provided for each

## APPENDIX C NS Constellation

The satellites involved in the Satellogic constellation are listed in the table below (April 2023). Satellites from which test dataset is observed are highlighted in yellow (4 satellites).

**Table 6-11: – List of operational NS Satellites<sup>8</sup>.**

Name	NORA ID	Int'l Code	Status
<a href="#">NUSAT-3</a>	42760	2017-034C	15/06/2017
<a href="#">SNUSAT-2</a>	43782	2018-099AA	03/12/2018
<a href="#">NUSAT-6 HYPATIA</a>	46272	2020-061A	03/09/2020
<a href="#">NUSAT-7 (SOPHIE)</a>	45017	2020-003B	15/01/2020
<a href="#">NUSAT-8 (MARIE)</a>	45018	2020-003C	15/01/2020
<a href="#">NUSAT-9 ALICE</a>	46828	2020-079B	06/11/2020
<a href="#">NUSAT-10 CAROLINE</a>	46832	2020-079F	06/11/2020
<a href="#">NUSAT-11 CORA</a>	46829	2020-079C	06/11/2020
<a href="#">NUSAT-12 DOROTHY</a>	46827	2020-079A	06/11/2020
<a href="#">NUSAT-13 EMMY</a>	46833	2020-079G	06/11/2020
<a href="#">NUSAT-14 HEDY</a>	46831	2020-079E	06/11/2020
<a href="#">NUSAT-15 KATHERINE</a>	46830	2020-079D	06/11/2020
<a href="#">NUSAT-16 LISE</a>	46840	2020-079P	06/11/2020
<a href="#">NUSAT-17 MARY</a>	46835	2020-079J	06/11/2020
<a href="#">NUSAT-18 VERA</a>	46836	2020-079K	06/11/2020
<a href="#">NUSAT-19 (ROSALIND)</a>	48905	2021-059AC	30/06/2021
<a href="#">NUSAT-20 (GRACE)</a>	48921	2021-059AU	30/06/2021
<a href="#">NUSAT-21 (ELISA)</a>	48920	2021-059AT	30/06/2021
<a href="#">NUSAT-22 (SOFYA)</a>	48919	2021-059AS	30/06/2021
<a href="#">NUSAT-23 (ANNIE MAUNDER)</a>	52168	2022-033M	01/04/2022
<a href="#">NUSAT-24 (KALPANA CHAWIA)</a>	52178	2022-033X	01/04/2022
<a href="#">NUSAT-25 (MARIA TELKES)</a>	52171	2022-033Q	01/04/2022
<a href="#">NUSAT-26 (M SOMERVILLE)</a>	52184	2022-033AD	01/04/2022
<a href="#">NUSAT-27 (SALLY RIDE)</a>	52172	2022-033R	01/04/2022
<a href="#">NUSAT-28 (ALICE LEE)</a>	52747	2022-057R	25/05/2022
<a href="#">NUSAT-29 (EDITH CLARKE)</a>	52764	2022-057AJ	25/05/2022
<a href="#">NUSAT-30 (MARGHERITA)</a>	52748	2022-057S	25/05/2022
<a href="#">NUSAT-31 (RUBY PAYNE-S)</a>	52752	2022-057W	25/05/2022
<a href="#">NUSAT-32 (ALBANIA-1)</a>	55064	2023-001BH	03/01/2023
<a href="#">NUSAT-33 (ALBANIA-2)</a>	55047	2023-001AQ	03/01/2023
<a href="#">NUSAT-34 (AMELIA EARHART)</a>	55045	2023-001AN	03/01/2023
<a href="#">NUSAT-35 (WILLIAMINA)</a>	55048	2023-001AR	03/01/2023

<sup>8</sup> <https://www.n2yo.com/database/?q=NUSAT-#results>

## APPENDIX D NS / MSI Instrument spectral channels

The NS / MSI instrument is sensing electromagnetic spectrum in four different spectral channels, the Blue, Green Red and NIR channels. Characteristics of these channels can be compared with ones from corresponding Sentinel-2 / MSI (S2 MSI) instrument.

As shown in Figure 6-6, differences exist for the Green, Red and NIR channels in particular regarding central wavelength (indicated in the figure aside channel name), spectral bandwidth and spectral shape. It is worth noting that, the NS NIR channel overlap O<sub>2</sub>-A-band molecular absorption (760 nm).

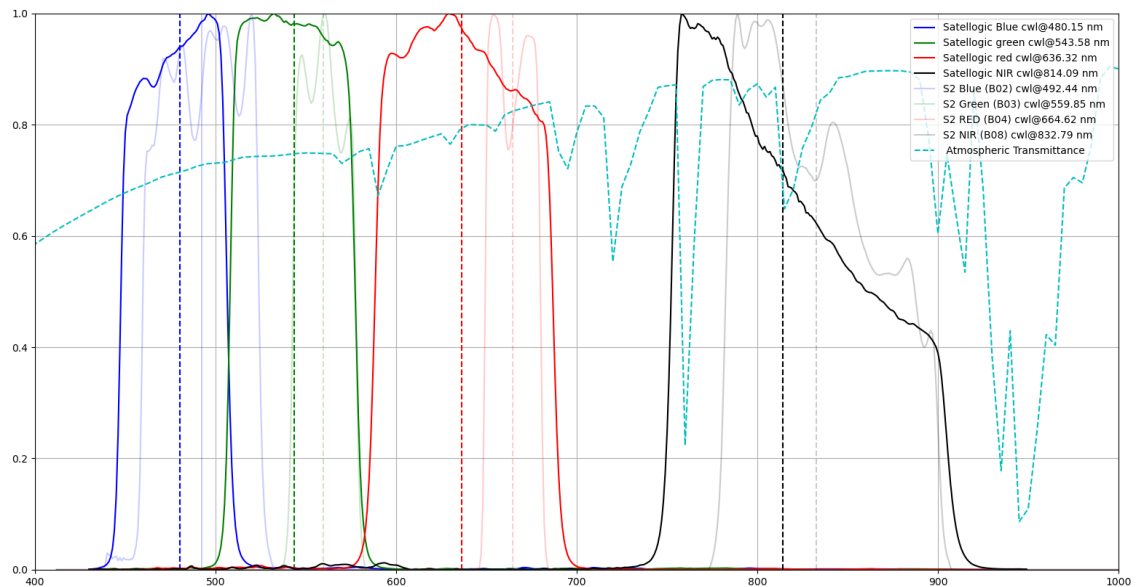


Figure 6-6: NS / S2 MSI Spectral bands comparison.

From a simulation point of view, by using instrument spectral responses and electromagnetic spectrum, it is possible to anticipate reflectance value. By considering another instrument (e.g., S2 / MSI), it is also possible to assess, depending on targets, how spectral differences between two instruments impact recorded value.

By considering a sample of spectrum, the spectral differences are modelled with a set of per channel coefficients called (SBAF). As shown in the formula below, the SBAF coefficient is an average value over the  $c$  parameter data sample.

$$\tilde{\rho}_{NewSat}^{\lambda} = c(\lambda) \times \tilde{\rho}_{S2A-MSI}^{\lambda}$$

For NS, simulations based on RadCalNet spectral database and ECOSTRESS spectral library have been done, and results are detailed just hereafter.

**It is worth noting that these results are from simulations and are here to support interpretation of radiometric calibration results detailed in Section 6.2.**

### RadCalNet spectral database

RadCalNet ([RD-17]) is an initiative of the Working Group on Calibration and Validation of the Committee on Earth Observation Satellites. The RadCalNet service provides satellite operators with SI-traceable Top-of-Atmosphere (TOA) spectrally-resolved reflectances to aid in the post-launch radiometric calibration and validation of optical imaging sensor data.

BOA / TOA Data over several years from the Baotou (B{S,T}CN), Gobabeb (GONA), La Crau (LCFR) , Railroad Valley Playa (RVUS) have been collected. Spectral information delivered with 10 nm Sampling interval for VNIR/SWIR channels (except Baotou) with quality information added.

The Table 6-12 list NS / S2 Simulated Percent differences and show that main differences exist for the Red channel, in particular for GONA / BSCN target (about 7 %) and in a less extent, these exist for the NIR channel in presence of vegetation (about 5% LCFR case).

**Table 6-12: NS / S2 Simulated Percent differences based on SBAF results (1 – c), RadCalNet.**

Site	Number of Spectrum	Blue	Green	Red	NIR
GONA	15444	0.84%	4.98%	7.23%	3.65%
LCFR	11908	-3.24%	-0.18%	4.45%	4.93%
BSCN	4056	1.04%	3.04%	7.90%	4.26%
BTCN	6643	-0.18%	-0.34%	3.43%	3.04%
RVUS	31694	1.54%	2.35%	4.60%	3.61%

As GONA land cover is very similar to Libya 4 land cover, results given in §6.3, the confidence intervals of SBAF percent differences are provided in Table 6-13.

**Table 6-13: NS / S2 SBAF percent differences, one-sigma interval confidence (GONA).**

	Blue	Green	Red	NIR
Maximum	1.35%	5.56%	7.56%	4.28%
Minimum	0.33%	4.40%	6.90%	3.02%

#### ECOSTRESS spectral library

The Version 1.0 of the ECOSTRESS spectral library<sup>9</sup> was released on February 2, 2018. This release added over 1100 new vegetation and non-photosynthetic vegetation spectra. The ECOSTRESS spectral library is a compilation of over 3400 spectra (2nm sampling interval) of natural and man - made materials.

The Figure 6-7 Left table lists SBAF percentage differences depending on spectral class. It shows that large differences are expected in the Red channel, in particular for vegetation / soil spectrum.

<sup>9</sup> <https://speclib.jpl.nasa.gov/>

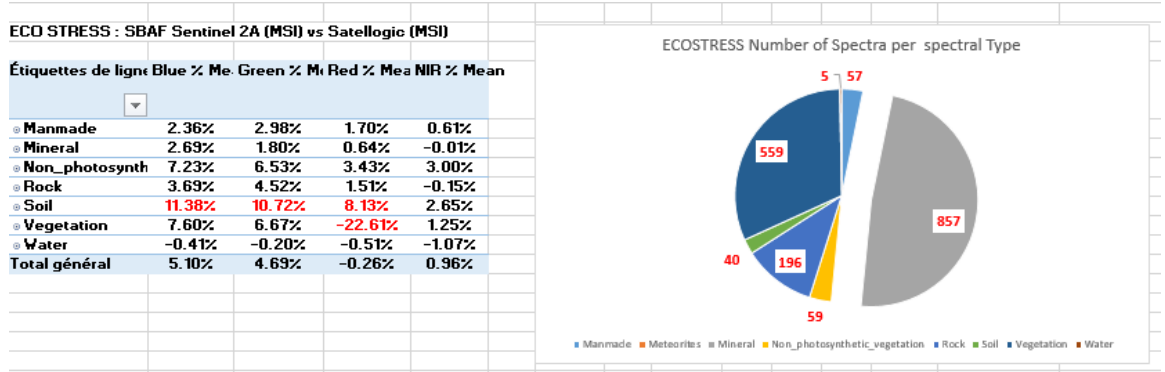


Figure 6-7: NS / S2 Simulated Percent differences based on SBAF results (1 – c), ECOSTRESS.

## APPENDIX E 74NS / MSI Instrument geometry

The NS / MSI satellite sensors are built in push-frame fashion. As shown in Figure 6-9, every channel (Blue, Green, Red, NIR) is recorded at the same time (same shot, Figure 6-8) as consecutive fixed frames with a small overlap. The distances between the images range between 150 – 300 meters depending on the satellite and the image GSDs (factor of satellite altitude and off-nadir angle). For a single channel, the image overlap is illustrated in Figure 6-9.

Furthermore, the NS / MSI satellite sensor is a single telescope; every channel has its own geometry. Thus, for a same location over the Earth, inter-band variations can be expected due to the perspective differences and un-removed camera optical distortions if exist.

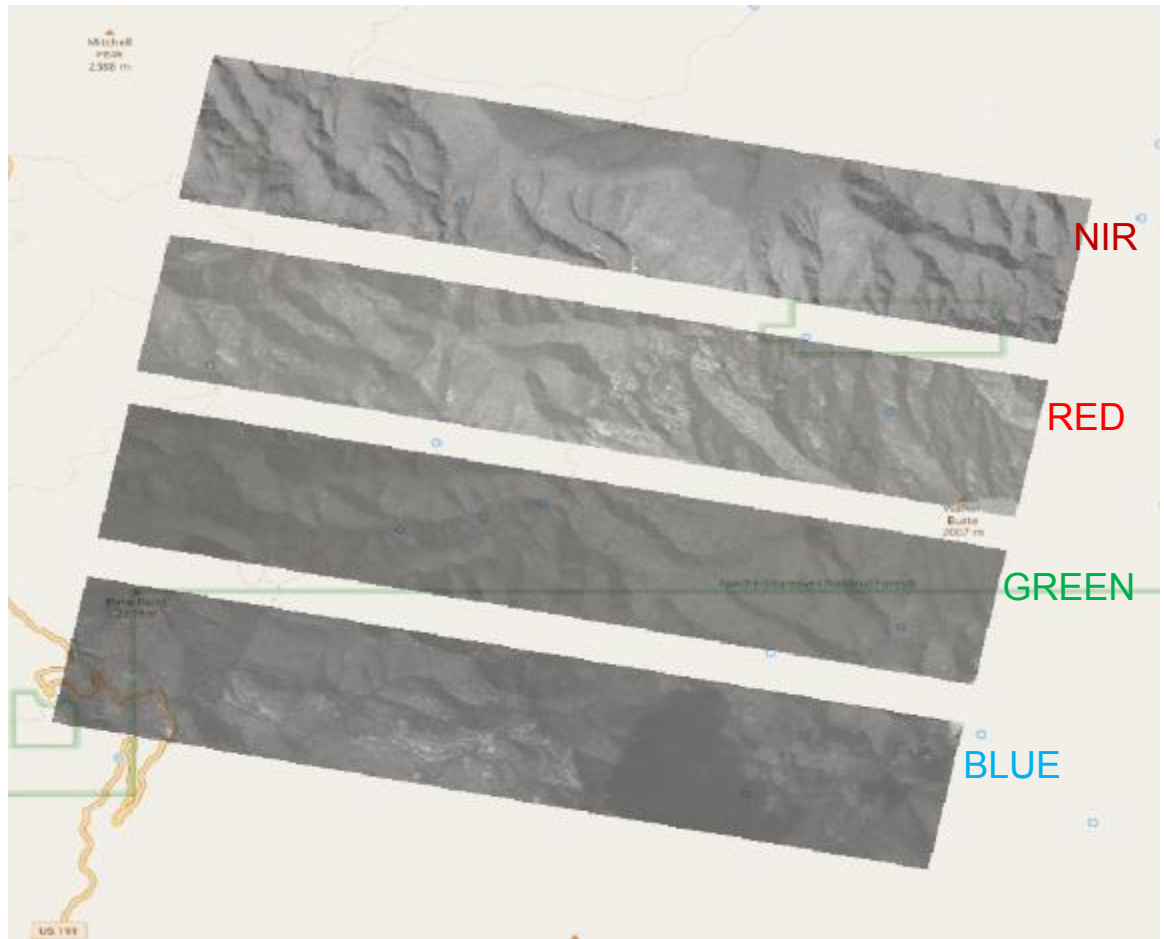


Figure 6-8 - One set of L1B image frames taken at the same time over Morenci, Arizona, USA. OpenStreetMap is used as basemap.



**Figure 6-9: Three consecutive L1B image frames (Red band) taken with a small overlap (ca. 150 pixels) over Morenci, Arizona, USA. Open Street Map is used as basemap.**

Our understanding is that the L1 and L3 processing is carried out based on image grids. The grids are defined for every acquisition compared to Sentinel-2 Military Grid Reference System (**MGRS**) that is fixed. An example of grids respectively defined for two acquisitions (Green, Pink colour) over Baotou is shown is given in Figure 6-10. A shift between two grids does not mean that the absolute geolocation accuracy is degraded. At tile level, an extra co-registration step is performed to reduce channel to channel mis-registration (Discussion with Satellogic team). It might introduce discrepancies, order of magnitude to be defined, in multi-temporal geolocation stability. It is worth noting that the impact of tiling can be appreciated in some KARIOS output figures shared within this document.



**Figure 6-10 - Baotou L3 images from SN30 from 18.06.2022 (left) and SN27 from 14.06.2022 (right) and their respective processing grids shown with pink (SN30) and yellow (SN27) polygons.**



**[END OF DOCUMENT]**